第52卷 第3期
2014年7月

古 脊 椎 动 物 学 报
VERTEBRATA PALASIATICA

pp. 265–302
figs. 1–9

A Late Miocene *Ursavus* skull from Guanghe, Gansu, China

QIU Zhan-Xiang DENG Tao WANG Ban-Yue

(*Key Laboratory of Vertebrate Evolution and Human Origins of Chinese Academy of Sciences*, *Institute of Vertebrate Paleontology and Paleoanthropology*, *Chinese Academy of Sciences* Beijing 100044 qiuzhanxiang@ivpp.ac.cn)

Abstract An almost complete *Ursavus* skull in association with its mandible is described. The skull was recently found from upper part of Liushu Formation in Linxia Basin. Its stratigraphic level and geologic age are correlated to the late Bahean ALMA/S, ~8 Ma. It represents a new species, here named *Ursavus tedfordi.* Cladistic analysis is conducted using the TNT software, based on a matrix of 11 taxa and 37 characters. The tree 5 of the 8 most parsimonious trees is chosen as the most reliable to reflect the phylogenetic history of the ursid clade. As the tree 5 shows, after divergence from the Oligocene-Early Miocene hemicyonids (*Cephalogale*), the ursid clade first yielded two stem-taxa: *Ballusia elmensis* and *B. orientalis*, the latter of which being an aberrant branch. Then, two major subclades emerged: one comprising *Kretzoiarctos*, *Agriarctos* and *Ailurarctos*, the other containing all *Ursavus* species and their descendants including all living bears (excluding *Ailuropoda*). *Kretzoiarctos* may not be the direct ancestral form of the giant panda as Abella and colleagues (2012) suggested, but the ancestral form of the lineage of *Indarctos* (+*Agriotherium* ?). Among the numerous *Ursavus* species, *U. tedfordi* is the most advanced and closest related to the living bears (excluding *Ailuropoda*) in morphology, however, might belong to a side-branch, judging by the autapomorphies possessed by it.

Key words China, Late Miocene, *Ursavus*, *Ailuropoda*

1 Introduction

In the last ten years or so, a number of skulls of *Indarctos*, *Agriotherium* and *Ursavus* have been collected from the Late Miocene deposits in the Linxia Basin. Since so far no complete *Ursavus* skull has ever been found and reported, and a number of questions pertainning to the origin, phylogeny and classification of the Ursinae are quite dependent on a better understanding of ancestral ursid members, especially the genus *Ursavus*, a well preserved skull of *Ursavus* was chosen as the subject of the first of a series of papers dealing with these ursid skulls.

The *Ursavus* skull was collected by Mr. Chen Shanqin, vice director of the Hezheng Paleozoological Museum, who came across the skull, still mostly embedded in rock, in

中国科学院战略性科技先导专项(编号：XDB03020104)、国家重点基础研究发展计划项目(编号：2012CB821906)和国家自然科学基金重点项目(编号：40730210)资助。

收稿日期：2013−12−30

Huaigou village of Guanghe County in July, 2006. Ancestral ursine fossils, especially those of *Ursavus*, are frequently found in Holarctic Miocene deposits, but mainly represented by teeth and fragmentary mandibles. The best specimen so far known is an anterior half of skull from the Island of Euboea (Greece), described in detail by Thenius in 1947. Another better preserved specimen is a skeleton from Shanwang, China, first described as *Ursavus orientalis*, but later reassigned to the genus *Ballusia*, of which only brief description of some teeth was reported by Qiu et al. in 1985. The present skull from Huaigou is thus the first and only complete skull with its associated mandible ever known of these early ursine bears.

From the same locality where this skull was found, rich fossils of typical North China *Hipparion* fauna were found. A preliminary list of the mammalian fossils includes: *Promephitis*, *Metailurus*, *Machairodus*, *Ictitherium*, *Hyaenictitherium*, *Hipparion*, *Chilotherium*, *Sinotherium*, *Palaeotragus*, and *Prosinotragus*. Of them *Promephitis* and *Sinotherium* have already been studied (Wang and Qiu, 2004; Deng et al., 2013). An age determination based on the evolutionary level of the *Promephitis* species was given as around 9−7 Ma, while on the other hand, 7 Ma was given by Deng et al., based on the presence of *Sinotherium lagrelii*.

The anatomical terms used by Jayne on cat (1898) and Davis on giant panda (1964) are adopted in general description of the skull in this paper, those proposed by Hunt (1974, 1977) for the ear region of ursids are selectively used when needed.

Abbreviations HMV, acronym for the vertebrate collection of the Hezheng Paleozoological Museum; IVPP, Institute of Vertebrate Paleontology and Paleoanthropology, Chinese Academy of Sciences; MPT, most parsimony tree.

2 Systematic description

Ursidae Fischer von Waldheim, 1817

Ursinae Fischer von Waldheim, 1817

***Ursavus tedfordi* sp. nov.**

(Figs. 1−8; Tables 1−5)

Etymology The species name is to cherish the memory of Richard Hall Tedford, the great North American Neogene biostratigrapher and paleomammalogist, who recently passed away on July 16, 2011.

Holotype HMV 1453, a cranium in association with mandible. The right paroccipital process, the hooks of the pterygoid processes, the left C, both P4s' protocones, and the antero-lingual corner of the right M1, were partly broken, and the left upper incisors were damaged (but reconstructed) during the preparation. The facial part of the skull is slightly compressed in left-dorsal–right-ventral direction, resulting in vertically shortening of the right orbit. The medial walls of both orbits are fractured. The specimen is the property of the Hezheng Paleozoological Museum (Hezheng, Gansu).

Type locality Huaigou village of Guanghe County (Zhao's Loc. 43 = IVPP Loc. LX 0029, 35°22′51.4″N, 103°26′54.4″E), Linxia Hui Autonomous Prefecture, Gansu Province.

Stratigraphic position and age Upper part of Liushu Formation, stratigraphically below the level containing the Yangjiashan local fauna. Late Bahean ALMA/S (Asian Land Mammal Age/Stage), better to be considered as around 8 Ma.

Diagnosis Large-sized *Ursavus* species, roughly intermediate between *Cephalogale minor* and *Selenarctos thibetanus* in size, proportion and morphology. The muzzle is short and broad compared with the back part of the skull. The sagittal crest is enormously high posteriorly, overhanging far beyond the nuchal surface. The cranial part is narrow compared with the facial part, expressed by the narrower medial pterygoid fossa, the basisphenoid-basioccipital region, the skull width across the mastoid processes and the braincase, maximum width of which is only slightly wider than that of the muzzle. The zygomatic bone extends posteriorly slightly beyond the anterior margin of the glenoid fossa. The posterior border of the bony palate is situated slightly posterior to the M2. The tympanic bulla is triangular in form, about equally long and wide, with a short tubular external auditory meatus. The ventral surface of the ectotympanic bone slopes ventrally toward its medial side, forming a curved longitudinal crest; whereas the entotympanics remain exposed, forming a longitudinal strip of irregular form. The small depression on the basisphenoid, supposedly housing the anterior end of the internal carotid artery loop, is present, but small. Mandible is robust, with its height under m1 far exceeding the length of m1, and its lower border is almost straight under the toothrow. The labial side of the symphysis is subvertical in lateral view, forming a 70° angle with the mandibular lower border, and a weakly expressed "chin" is present. Premolars strongly reduced in size and button-shaped. P1/p1 larger than P2/p2. P2/p2 in the initial stage of becoming single-rooted, P3/p3 double-rooted. P4 carnassial blade formed by metastyle and the posterior half of paracone. Its protocone is strongly reduced, situated opposite to or slightly anterior to the carnassial notch. It is tri-rooted, with its postero-buccal and lingual roots superficially coalesced. M1 about equally long and wide, considerably longer than P4. M2 longer, but narrower than M1, with a short talon. The metaconid of m1 is a tiny tubercle, situated postero-lingual to protoconid and situated much higher than the small doubled entoconid. The hypoconid is voluminous, occupying 2/3 width of the talonid, and only slightly lower than entoconid. The m3 is oval in shape, about 2/3 as long as m2. Enamel wrinkles hardly developed on cheek teeth.

Description HMV 1453 is apparently of a fully adult male individual. All the incisors, especially the upper, are heavily worn, the carnassial blades of both P4 and m1 are considerably so, while the other teeth remain almost unworn. Most of the bone sutures are fused. On the skull roof only the internasal, naso-premaxillar, naso-frontal, fronto-maxillary and fronto-lacrymal sutures are visible. According to Marks and Erickson 1966's investigation into the age determination in living American black bears (*Ursus americanus*), the tooth wear pattern and the suture-closing stage observed in HMV 1453 roughly correspond to 8 year old

individuals of the latter species. In combination with the excessive sagittal crest, the HMV 1453 skull is reasonably to be assigned to a fully adult male individual of *Ursavus tedfordi*.

Cranium (Figs. 1−5; Table 1) **Dorsal view** (Fig. 1): The muzzle is broad compared with the cranial portion of the skull. Its maximum width across the canines is the same as the width

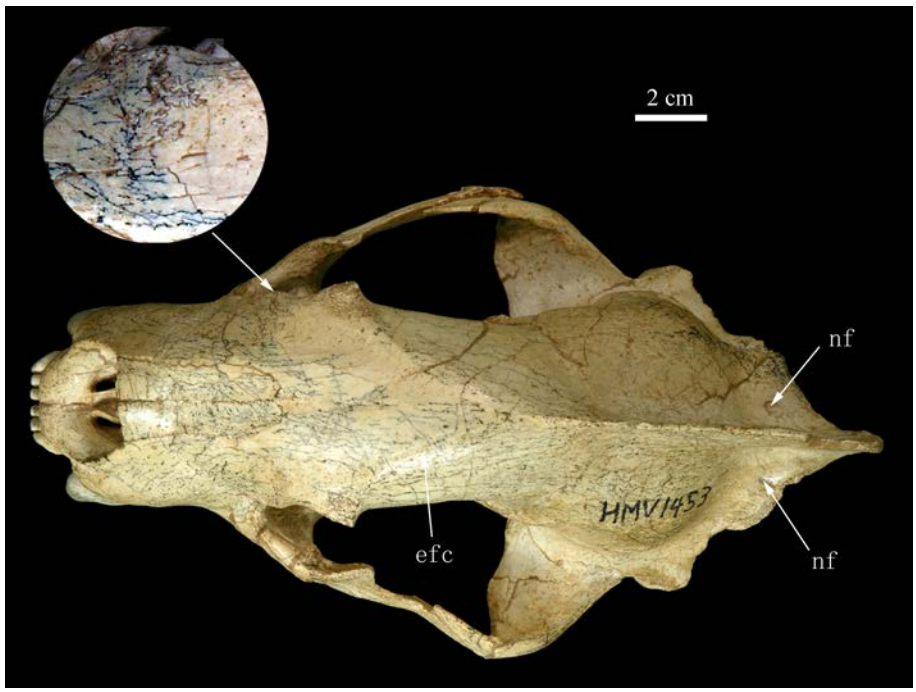

Fig. 1 *Ursavus tedfordi* sp. nov., HMV 1453 (holotype), skull, dorsal view
Abbreviations: efc. external frontal crest-line; nf. nutrient foramen

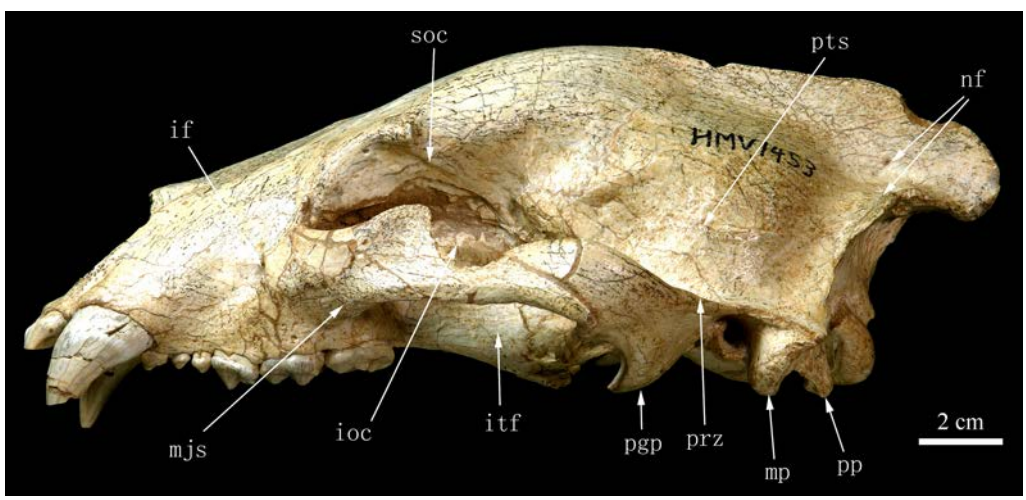

Fig. 2 *Ursavus tedfordi* sp. nov., HMV 1453 (holotype), skull, left lateral view
Abbreviations: if. infraorbital foramen; ioc. inferior orbital crest; itf. infratemporal fossa; mjs. maxillo-jugal suture; mp. mastoid process; nf. nutrient foramina; pgp. postglenoid process; pp. paroccipital process; prz. posterior root of zygoma; pts. parieto-temporal suture; soc. superior orbital crest

measured immediately posterior to the postorbital processes (61 mm) and about the length from the orbit's anterior rim to the anterior border of the C alveolus (63 mm). The nasals are elongated, slightly narrowed posteriorly, so that their lateral borders scarcely convergent posteriorly. They are 21 mm wide and 50 mm long measured at their mid-length. Their anterior margin is almost straight, with hardly discernible median nasal spine and external nasal processess, while the posterior border of each nasal is rounded, the posterior-most point of which is slightly posterior to the most posterior point of the fronto-maxillary suture. There is a tiny sagittal spine of the frontal bones wedged between the nasals. The nasals are mostly flat transversely, with only the anterior part weakly up-turned and convex. In the middle part of the nasals a number of tiny nutrient foramina are variously present, but a larger sagittal one, which is a short distance away from the anterior end, is present here, as in all living bears. The internasal, naso-premaxillary and naso-frontal sutures are clearly shown. However, the maxillo-premaxillary suture is obliterated. The naso-frontal suture forms a W-shaped figure. The nasal process of the frontal bones, inserting between the nasal and maxilla, is short, ~14 mm long, with a broad anterior end (~4 mm wide), lying above the anterior border of the orbit. The fronto-maxillary suture is less clearly shown, however, with its lateral half so strongly wrinkled that a kind of "ammonite suture" is formed (see the insert in Fig. 1). The interfrontal suture is almost completely obliterated. The dorsal surface of the interorbital region is rather flat, so that the upper orbital rim is only slightly lower than the dorsal profile of the frontal (Fig. 2). The interorbital width of the frontal is about as wide as the muzzle across the canines. The posterior part of dorsal surface of the frontals is strongly arched transversely and longitudinally, forming the apex of the skull profile. The postorbital process of the frontal forms a small angular protuberance, with its posterior side sub-normal to the cranium long axis, while its anterior side converging anteriorly. A scarcely discernible crest-line represents the external frontal crest (Fig. 1 efc), or temporal ridge (term used by Jayne, 1898:477), which extends from the postorbital process medio-posteriorly, merging into the unified sagittal crest 18 mm anterior to the mid-point of the fronto-parietal sutures. The postorbital constriction is slightly narrower than the muzzle. The braincase is convex, with its maximum width near the level of the external auditory maeatus, reaching ~73 mm. A pair of large nutrient foramina (Fig. 1 nf) are located bilaterally to the sagittal crest and at the supero-posterior corners of the parietal bones. The sagittal crest is particularly developed, ~110 mm long, extending posteriorly far beyond the nuchal surface. The horizontal shelf formed by the posterior root of the zygoma and the portion of the temporal above and posterior to the mastoid process is present, but markedly narrower than in the living bears.

Lateral view (Fig. 2): In general, the skull is characterized by having a domed frontal region, a long and high sagittal crest.

The apex of the profile is situated at the posterior 1/3 of the frontals. Anterior to the apex the profile line slopes down markedly, while posterior to the apex the profile line slopes gently. The sagittal crest extends posteriorly far beyond the posterior surface of the occipital, ~30 mm

Table 1 Measurements and comparison of skulls of *Ursavus* and some living bears (mm)

	Ursavus		*Ursus*			
	tedfordi	*ehrenbergi*	*thibetanus*		*arctos*	
	Huaigou HMV 1453 Holotype	Almyropotamus Thenius, 1947	IVPP OV 484	Gao et al., 1987	IVPP OV 489	Gao et al., 1987
1. Vertex L (prosthion−inion)	250		290		350	
2. Condylobasal L (prosthion−posterior border of condyles)	215		~270	235−413 [290.9] (260−315)	332	258−362 [305.3] (258−418)
3. Basilar L (prosthion basion)	204		250		310	
4. Facial L (prosthion−mid-point of postorbital constriction)	125		~165		215	
5. Muzzle L (prosthion−anterior orbital rim)	67		94		125	
6. Nasal L (along sagittal line)	50		66		100	
7. Cranial L (inion−mid-point of postorbital constriction)	125		~125		140	
8. Palatal L I (mid-point of I1' s alveolar borders−posterior border of palate)	98		142	122.3−172.3 [146.6]	180	128−190.8 [158.9]
9. Palatal L II (posterior borders of incisive foramina−posterior border of M2)	66	88.8	86		115	
10. Sagittal distance between M2 and posterior border of palate	19		27		37	
11. Maximum skull W at zygomatatic arches	140		~180	141.4−240.1 [179.4] (163−228)	205	140.5−198.4 [178.9] (147−277)
12. Skull W at mastoid processes	99		142		158	
13. Palatal W between the M2's	34.5	49.6	38.3		53	
13/9 (%)	52.3	55.9	44.5		46.1	
14. Muzzle W at C	61	66.5	65		78	
15. Palatal W between C	35	40.7	33		46	
16. Muzzle H at around P3	40	53.8	52		65	
17. H of occiput (inion−mid-point of line connecting lower borders of condyles)	70		~80		95	

Note: Means in [ ]; measurements of Novikov, 1956 in ( ); L. length; W. width; H. height.

overhanging the occipital condyles. The lateral margin of the nasal aperture is predominantly formed by the premaxillary, with the nasal hardly seen from lateral side, owing to the flatness of the nasal bone. The infraorbital foramina (Fig. 2 if) are located above the boundary between the P4 and M1, but they are different in form. On the left side the foramen is single and oval in anterior view (8 × 4 mm), while the right one is doubled, with a combined height of 9 mm. The left incomplete bony ring of the eye socket is little deformed and retains its original form. The bony ring is roughly rounded, about equally high and long, with its antero-dorsal border weakly curved, lacking an angled dorso-posterior corner as in living bears. The anterior border of the orbit is situated above the posterior part of the M1. The medial walls of the orbital cones are fractured variously on both sides, but a considerably reliable reconstruction can be obtained owing to the mutually supplementary state of preservation. The superior orbital crest (*crista*

orbitalis superior; for terminology see Davis, 1964:49) is weakly expressed in its antero-superior half (Fig. 2 soc). It is represented by a weak ridge sending from below the postorbital process of the frontal postero-inferiorly, attenuating toward the middle of the crest, so that the crest is only 13 mm long. Its postero-inferior half forms a clear stepped structure, strongly depressed antero-inferiorly around the orbital fissure (sphenoidal fissure of Jayne, 1898) and prominently bulged postero-superiorly, forming the anterior boundary of the temporal fossa. The inferior orbital crest (*crista orbitalis inferior*; Davis, 1964:49) is hardly distinguishable in its posterior 2/3 (Fig. 2 ioc). A fine, but sharp crest, ~25 mm long, can be clearly seen on the right side of the skull, which originates from the external 1/3 of the posterior border of the lacrimal fossa. The anterior end of the orbital cone, where several important foramina are present, have been prepared on the right side of the skull. The lacrimal fossa is situated at the antero-inferior corner of the orbital cone. It is very large, and oval in form. No separate *fossa muscularis* can be found (often in form of a separate foramen in living bears). Neither can it be for certain that the *fossa muscularis* is confluent with the lacrimal fossa. The ethmoidal and optic foramina can hardly be located for certain because of the fracture of the middle part of the medial walls of both orbital cones. Posteriorly, the orbital fissure is clearly shown on the left side of the skull. It comprises two foramina, which are situated in a large common opening, but well separated from each other by a septum. They are roughly rounded in form, of about the same size.

The infratemporal fossa is large compared with the orbital cone (Fig. 2 itf). They are vaguely separated from each other in their posterior 2/3. At the anterior end of the infratemporal fossa, just below and lateral to the lacrimal fossa, there is the posterior opening of the infraorbital canal, which is slightly larger than the lacrimal fossa, and roughly triangular in form. At about the same level, ~20 mm posterior and medial to the infraorbital canal, there is a single rounded foramen, which lies above and slightly posterior to the M2. Davis (1964:48) called a similarly positioned foramen in giant panda the common foramen for the sphenopalatine and pterygopalatine foramina and pointed out that these two foramina are separate in living *Ursus* species. Jayne (1898: 475) called these two foramina in *Felis catus* the posterior palatine (the anterior one) and sphenopalatine foramina (the posterior one). Here we follow Davis' usage, call it the common foramen for sphenopalatine and pterygopalatine foramina. The middle and posterior part of the infratemporal fossa is convex vertically, forming a short crest, ~10 mm long, above the hamular process of the pterygoid bone. At the posterior end of the infratemporal fossa there is an alisphenoid canal. It anterior opening lies lateral to the foramen rotundum, separated from the latter by a clear septum. In fact all the three foramina, the orbital fissure, the foramen rotundum and the anterior opening of the alisphenoid canal, are situated side by side, and share a large common depression. The posterior opening of the alisphenoid canal is situated in the anterior end of the common fossa shared with the *foramen ovale*, which is situated slightly posterior to the anterior margin of the glenoid cavity. This common fossa is situated at about the same level as the base of the glenoid cavity.

The zygomatic arch is weakly arched, especially in its posterior part. The maxillo-jugal suture (Fig. 2 mjs) is well preserved on the right side, strongly zigzag in form, extending from the anterior-most point of the orbital rim postero-ventrally, forming a faint tubercle at its postero-inferior end. The lower margin of the zygomatic process of the maxilla, i.e., the anterior root of the zygomatic arch, begins above the anterior half of the M2. The postorbital process of the jugal is larger than that of the frontal, lobe-shaped. The middle part of the zygomatic arch is very thin and narrow. The jugal bone extends posteriorly even slightly beyond the anterior margin of the glenoid fossa.

The temporal fossa is well delineated by the sagittal and lambdoidal crests and the sharp lateral ridge of the posterior root of the zygoma (Fig. 2 prz). Anteriorly, the boundary of the temporal fossa is less clearly defined: both the external frontal crest-line (Fig. 1 efc) and the superior orbital crest (Fig. 2 soc) are not so prominent as in living bears. The parieto-temporal suture is largely fused, but on the left side of the cranium a roughly horizontal ridge (Fig. 2 pts) represents this suture, apparently serving as the attachment area for the tendinous sheet of *M. temporalis*. The sagittal crest rapidly increases its height posteriorly, forming a high vertical plate, reaching 32 mm at its highest part. Its posterior end extends ~25 mm beyond the nuchal surface so that the lambdoidal crest becomes strongly curved seen from lateral side. Near the turning point from horizontal to vertical part of the lambdoidal crest one or two conspicuous nutrient foramina (Fig. 2 nf) are present on each side of the cranium, but the foramina are not

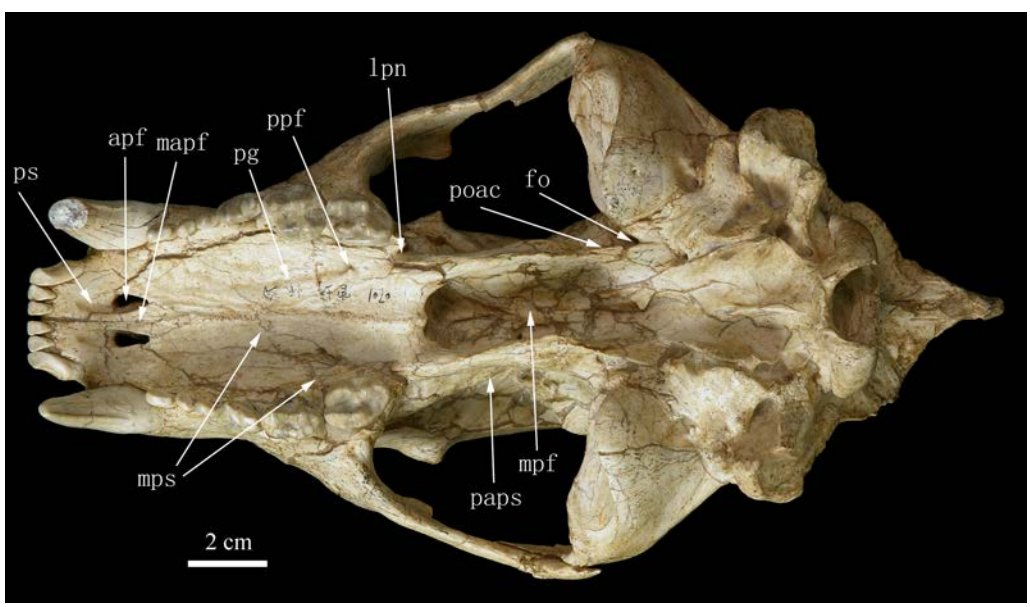

Fig. 3 *Ursavus tedfordi* sp. nov., HMV 1453 (holotype), skull, ventral view
Abbreviations: apf. anterior palatine foramen; fo. foramen ovale; lpn. lateral palatine notch; mapf. median anterior palatine foramen; mpf. medial pterygoid fossa; mps. maxillo-palatine suture; paps. palatine-alisphenoid-pterygoid strut; pg. palatine groove; poac. posterior opening of alisphenoid canal; ppf. posterior palatine foramen; ps. palatine fossa

symmetrically situated. The crest situated posterior to the posterior root of the zygomatic arch extends postero-ventrally, so that a sub-rectangular angle is formed with the lambdoidal crest. The postglenoid, mastoid processes are robust, while the paroccipital process is comparatively small (Fig. 2 pgp, mp and pp). The lower extremities of the three processes are roughly aligned in the same horizontal line.

Ventral view (Figs. 3, 4): The skull is characterized by having a particularly short palate, the more straight zygomatic arches and comparatively narrow cranial part of the skull posterior to the glenoid condyles.

The palate is narrow and short. It is vaulted, with its deepest part situated between the P4−M1. In the anterior part of the palate there is a pair of palatine fossae (Fig. 3 ps), which are long and lanceolate in form, parallel with each other. The posterior halves of the fossae are pierced by the paired anterior palatine foramina (Fig. 3 apf). A tiny median anterior palatine foramen (Fig. 3 mapf) lies between the fossae slightly anterior to their posterior ends. Only the median part of the premaxillo-maxillary suture is observable. This suture starts from the posterior end of the anterior palatine foramen, extending postero-medially so that the two palatal processes of the premaxillaries penetrate deep into the maxillary bones, ending at the level of the anterior end of the P2. The maxillo-palatine suture (Fig. 3 mps) forms a wide arch with its anterior-most point reaching the level of the P4 protocone. The posterior palatine foramina (Fig. 3 ppf) are situated slightly posterior to the anterior border of the M2, but always within the palatine bones. The palatine grooves (*sulcus palatinus*) linking the anterior and posterior palatine foramina are faint, especially in their anterior parts (Fig. 3 pg). The posterior border of the palate [Davis' term (1964:51), but Jayne (1898:321) called it the posterior border of the horizontal plate of the palatine bone] extends 7 mm posterior to the M2, with a clear median spine (Jayne: posterior nasal spine). No vomer can be seen above the median spine, indicating the vomer does not extend to the level of the choana. A small lateral palatine notch (Davis' term) is present on the lateral border

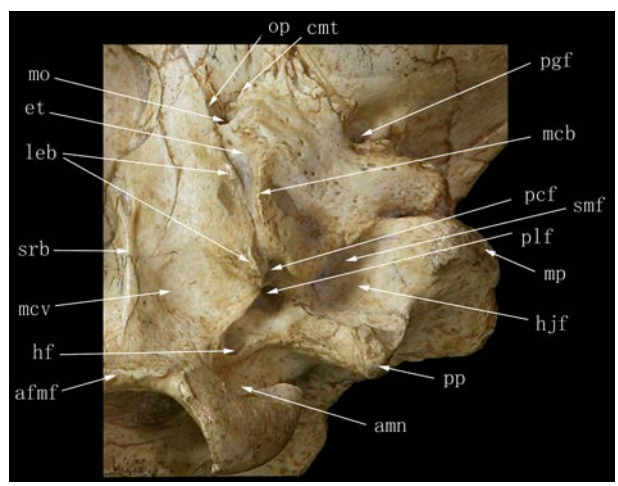

Fig. 4 *Ursavus tedfordi* sp. nov., HMV 1453 (holotype), skull, left half of basioccipital region, ventral view

Abbreviations: afmf. ante-foramen magnum facet; amn. antero-medial notch of condyle; cmt. *canalis musculotubarius*; et. entotympanic; hf. hypoglossal foramen; hjf. hyojugular fossa; leb. lateral edge of basioccipital; mcb. medial crest of bulla; mcv. attatchment area for *musculus rectus capitis ventralis*; mo. antero-medial opening of bulla; mp. mastoid process; op. oval pit for lodging internal carotid artery; pcf. doubled posterior carotid foramen; pgf. postglenoid foramen; plf. posterior lacerated foramen; pp. paroccipital process; smf. stylomastoid foramen; srb. sagittal ridge of basioccipital

of the horizontal plate of the palate, situated slightly internal to the posterior ends of the M2 (Fig. 3 lpn). The medial pterygoid fossa (Jayne, 1898:466) or nasopharyngeal fossa (Davis' term (1964:51) is narrow, long and deep, so that the fossa is about equally high and wide (Fig. 3 mpf). No prominent median keel formed by the vomer is clearly shown. The palatine-alisphenoid-pterygoid strut (Fig. 3 paps) is stout, with its lateral surface convex and sculptured in its posterior half. Posterior extremeties of both pterygoid hamuli are broken, however, they seem to be situated more anteriorly relative to the glenoid cavities. The posterior edge of the strut ascends towards the *canalis musculotubarius* of the tympanic bulla, forming a high wall to separate the *foramen ovale* (Fig. 3 fo) and the posterior opening of the alisphenoid canal (Fig. 3 poac) from the medial pterygoid fossa.

The ventral side of the zygomatic arch is thin and ridge-like. The attachment area for the masseter forms a long strip along the lateral side of the ventral border. The medial end of the glenoid cavity (Davis: mandibular fossa) descends scarcely more ventrally than the basal portion of the alisphenoid bone bearing the foramen ovale and the alisphenoid canal.

The basioccipial and basisphenoid bones are completely fused on ventral side so that no boundary between them can be traced. If the basioccipito-basisphenoid suture lies around or slightly posterior to the line connecting the antero-medial corners of the tympanic bullae as usual in the living bears, the ventral side of the basioccipital is roughly hexagonal in form, with the anterior bilateral borders much longer than the posterior ones. The basioccipital is deeply hollowed centrally, with their lateral edges which overlap the entotympanic parts of the bullae, turning sharply ventrally (Fig. 4 leb). The maximum depth of the hollow is ~10 mm. A blunt sagittal ridge on the basioccipital attenuates anteriorly and vanished before reaching to the anterior end of the basioccipital bone (Fig. 4 srb). The paired attachment scars for the *M. rectus capitis ventralis major* (or *M. longus capitis*) are large, but poorly delineated, while those for the *M. rectus capitis ventralis minor*, situated posterior to the former, are smaller, but form a pair of better delineated depressions (Fig. 4 mcv).

The outline of the tympanic bulla plus the external auditory meatus resembles a fan with a pedicle. The ventral surface of the bulla is rather flat, provided with a sharp crest near the medial side of the bulla (Fig. 4 mcb). The crest is sinuous, with its posterior 2/3 weakly convex medially and the anterior 1/3 strongly concave. Thus, between the sinuous crest and the lateral border of the basioccipital is an opaque bony groove of irregular form, suddenly widening anteriorly. As evidenced by Hunt's study of the bears, this part of bone could be the entotympanics (Hunt, 1974: pl. 4, 16). Therefore, even in adult individual the entotypmpanics are clearly exposed on ventral side of the basicranium in *Ursavus tedfordi* (Fig. 4 et). At the antero-medial corner of the bulla there are two large foramina: a larger medial opening situated anterior to the entotympanic and a smaller lateral one situated anterior to the ectotympanic. The medial opening (Fig. 4 mo) is very deep, leading to the foramen lacerum medium, and an oval pit (Fig. 4 op) can clearly be seen anterior to this foramen. This pit extends anteriorly ~4.5 mm beyong the ventral border the medial foramen. According to Hunt (1974:36), this

pit is the housing place for the anterior 180º turn-around end of the double-looped internal carotid artery. The lateral foramen is smaller and dorso-ventrally compressed. This should be the Eustachian opening. Davis (1964:51-52), called a similarly positioned opening the "entrance to the *canalis musculotubarius*", because of the confluence of both the *semicanalis M. tensoris tympani* and the *semicanalis tubae auditivae* (Fig. 4 cmt). The anterior process of the ectotympanic is wide and irregular in form, overlapping the basal part of the alisphenoid and the postglenoid process of the temporal. The postglenoid foramen is large, situated at the level where the external auditory meatus starts (Fig. 4 pgf). At the postero-medial corner of the bulla and the posterior part of the most ventrally extended lateral edge of the basioccipital is a large and deep depression containing three foramina, the upper two of which are small and should be the doubled posterior carotid foramen (Fig. 4 pcf), and a much larger lower one, which should be the posterior lacerated foramen (Fig. 4 plf). The hypoglossal (or condyloid) foramen (Fig. 4 hf) is small, situated in a vaguely delineatd common depression with the posterior lacerated foramen, separated from the latter by a blunt saddle-shaped prominence. Postero-lateral to the bulla a vast depression, believed by Davis (1964:52) highly characteristic of most of the ursoid animals and a new term was created for it, hyojugular, is well developed (Fig. 4 hjf). However, it is here comparatively small, but very deep. At its antero-medial end, immediately postero-lateral to the bulla, is the stylomastoid foramen (Fig. 4 smf), with a weakly delineated groove on the medial surface of the mastoid process. The hyoid fossa can not be clearly separated from the stylomastoid foramen. The postero-lateral surface of the hyojugular fossa slopes steeply, bordered by a crest linking the mastoid and paroccipital processes, although the middle part of the crest is very weakly expressed. Postero-medially, the hyojugular fossa is bordered by a ridge connecting the paroccipital process and the posterior end of the bulla.

The anterior border of the condyle is markedly notched near its medial end (Fig. 4 amn). There is a short but wide facet placed immediately anterior to the *foramen magnum* and between the condyles, but separated from the latters by narrow grooves (Fig. 4 afmf).

Occipital view (Fig. 5): The external surface of the occipital plate of the skull is characterized by a very high and overhanging posterior end of the sagittal crest (inion) and the little emarginated lambdoidal crest at the level slightly above the mastoid foramen.

The occipital surface without the overhanging inion is in fact more or less vertical, especially so is the supraoccipital part. Its general contour is triangular, with particularly widened base represented by the lateral borders of the mastoid processes. The external occipital crest (Davis: median nuchal line) is prominent in its upper half, fading out before reaching the foramen magnum (Fig. 5 eoc). This crest is flanked by a pair of broad depressions, which are punctuated by numerous tiny nutrient foramina. These broad depression may be the attachment areas mainly for the fleshy *M. rectus capitis dorsalis*. About 6 mm away from the crest and immediately below the lambdoidal crest are a pair of conspicuous scars of small size. Judging from their position (see Davis, 1964:169), the scars might be the attachment places for the *M. biventer cervicus*, which might become partly tendinous. The paired mastoid foramina

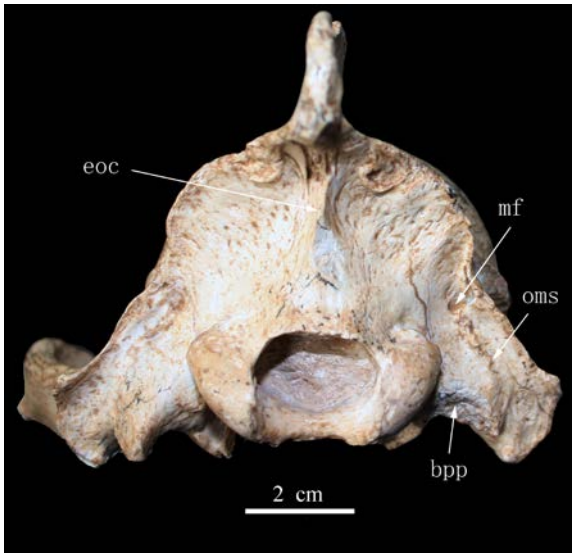

Fig. 5 *Ursavus tedfordi* sp. nov., HMV 1453 (holotype), skull, occipital view
Abbreviations: bpp. broken paroccipital process; eoc. external occipital crest; mf. mastoid foramen; oms. occipito-mastoid suture

(Fig. 5 mf) are small and situated slightly above the level of the upper border of the *foramen magnum*, at the upper ends of the occipito-mastoid sutures (Fig. 5 oms), which can be clearly traced on the right side. The *foramen magnum* is oval in shape, wider than high, without cleft or tubercles at the middle part of its upper border. The occipital condyles are weakly diagonally canted. Ventrally they are widely separated.

Mandible (Fig. 6; Table 2) The mandible is complete, with only its left angular process slightly deformed. The left hemimandible shows bone resorption between and beneath the m1 and m2 on labial side.

The mandible is sturdy in general appearance, with the two hemimandibles firmly united at the symphysis, although the symphysial suture is still clearly shown. The labial surface of the symphysial portion is rather flat in its upper part, perforated by a number of tiny foramina and a pair of larger ones which are ~10 mm under the i2 alveolar borders. Toward the lower end the labial surface of the symphysis becomes carinated, forming a weak “chin” which can clearly be seen from the lateral side. The anterior part of the lingual surface of the symphysis is almost horizontal (see Fig. 8 lss), extending to the level around the posterior end of the p1 (on left hemimandible) or the anterior half of the p2 (on right side), then turning sharply downward. The horizontal ramus, or the body, is deep and thick, with its ventral border almost straight antero-posteriorly. It is slightly higher under the premolars (~37 mm) than under the molars (33 mm). Anteriorly, the lower border of the body forms an angle of ~70° with the labial side of the symphysis, while posteriorly, it curves upwards around the inconspicuous “marginal process” (term used by Davis, 1964:61).

The marginal process lies behind the m3 and inflects lingually so that it can hardly be distinguished in lateral view (Fig. 6 mp), but clearly shown on lingual side and can be seen from above (see Fig. 8 mp). The thickest part of the ramus (17 mm) lie in its lower portion just behind the symphysis, while the next thickest point (15 mm) lies in the middle of the ramus below the m2. Mental foramina on the buccal surface of the ramus are generally small and roughly at the mid-height of the body, but different in position, number and size on the two hemimandibles. On the left one there are four (Fig. 6 mf), below the p1-p2, p3, p4, and the anterior half of the m1 respectively, with the third one being the smallest (nutrition foramen?).

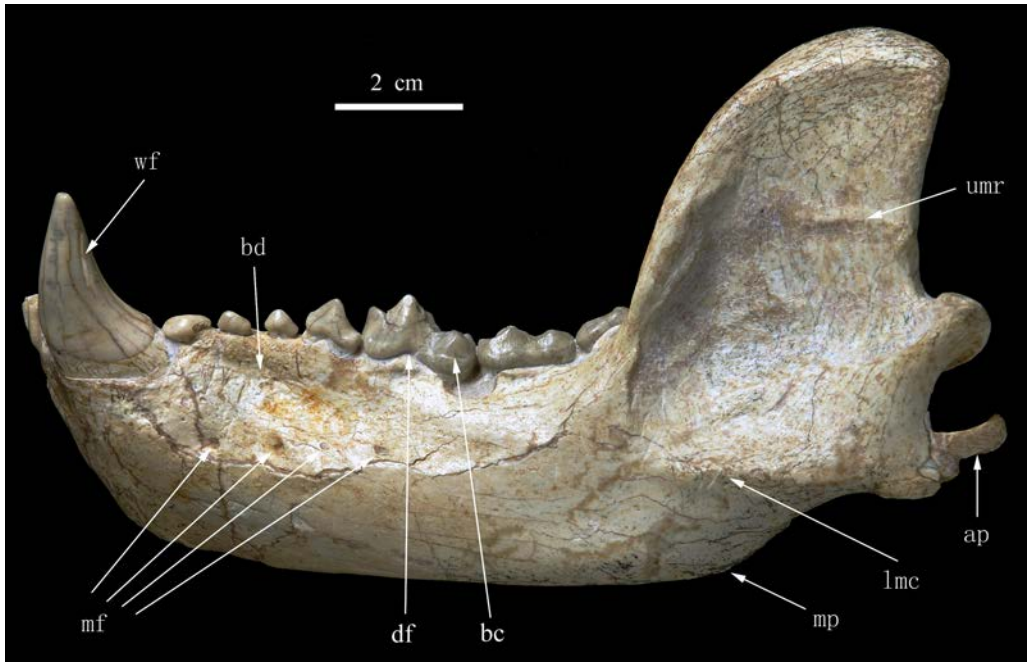

Fig. 6 *Ursavus tedfordi* sp. nov., HMV 1453 (holotype), mandible, left lateral view
Abbreviations: ap. angular process; bc. buccal cingulum; bd. buccal depression; df. dorsal flexion; lmc. lower masseteric crest; mf. mental foramina; mp. marginal (digastric) process; umr. upper masseteric ridge; wf. wear facet caused by upper canine

On the right hemimandible there are only three, below the posterior end of the p1, p3 and p4-m1. A remarkable, deep and broad depression on buccal side extends from underneath the p1 postero-inferiorly, fading out below the anterior half of the m2 (Fig. 6 bd). Below this depression the body is strongly bulged, forming the thickest portion of the ramus.

The coronoid process is rather wide in its upper part so that its anterior and posterior borders tend to be parallel, slanting weakly backward, without forming a hook-like postero-dorsal angle as in living bears. The masseteric fossa is bordered by an anterior blunted ridge and a lower crest as usual in ursines without premasseteric fossa. Both the ridge and the crest attenuate toward their junction. The junction is roughly rectangular in form, lies slightly above the mid-depth of the ramus. The lower masseteric crest (Fig. 6 lmc) extends posteriorly to form the sharp ventral crest of the angular process. The surface of the masseteric fossa is not particularly rugose, and is marked by several transverse masseteric ridges (cristae massetericae). The upper-most ridge is better shown (Fig. 6 umr). It strats from the lower 1/3 of the posterior edge of the coronoid process, extending anteriorly, forming a dorsally convex line, to which the tendinous sheet of the temporal muscle should attach. The middle ones are faint. These may serve the attachment for the tendinous sheets of the zygomaticomandibular muscle. The lowest boundary crest is the most prominent crest leading posteriorly to the lower border of the lateral side of the angular process (better seen on right hemimandible). The crest becomes wider and rougher in its middle part, serving evidently the attathment of the tendinous

sheets of the masseter muscle. The condyloid process is generally constructed as usual for a typical carnivore animal. The condyle is semicylindrical in form. The lateral edge of the posterior border of the coronoid process goes almost to the middle of the semicylinder, making the external half of the condyle longer than the inner half. The angular process (Fig. 6 ap) is prominent, forming the most posterior point of the hemimandible. It lies definitely higher than the lower border of the hemimandible. It is long and hook-like, with its cross-section triangular in shape. The dorsal and the medial surfaces of the angular process are concave transversely. Together with an insertion scar situated anterior to the angular process, these two concave surfaces serve the attachment of the internal pterygoid muscle. On the lingual surface of the hemimandible, the madibular foramen is situated roughly in the middle of the line drawn from the posterior border of the m3 to the posterior border of the hemimandible below the condyle. The marginal (or digastric) process is noticeable as a small knob on lingual side of the lower border below the mandibular foramen (see Fig. 8 mp). From this digastric knob a crest extends

Table 2 Measurements and comparison of mandibles of some primtive ursid taxa (mm)

	Ballusia		*Ursavus*	
	elmensis		*tedfordi*	*brevirhinus*
	Holotype		Huaigou	Holotype
	Stehlin, 1917	Dehm, 1950		Hofmann, 1887
Hemiandible L (base of i1−post. border of condyle)			157	
H of horizontal ramus posterior to p3	16.7*	15.4*	38	27
H of horizontal ramus at m2−m3	20*	17.5*	34	29
H from top of ascending ramus to bottom of horizontal ramus			85	
H from top of condyle to bottom of angular process			33	
L of p1−p4			33.2	26.4
L of m1−m3	26.3*		45	35.7
L of p1−m3		56*	77	61

Note: * measured on figures by the authors of the present paper; L. length; H. height.

antero-externally, gradually merging with the lower border at the level below the anterior border of the massetric fossa.

Upper dentition (Fig. 7; Tables 3, 4) The three incisors on each side are tightly appressed to each other, but leaving a cleft between the two I1's. The I1 is slightly smaller than the I2. Both I1 and I2 are heavily worn. The enamels on the lingual sides have been almost worn out on both incisors, while on labial side the height of the remaining enamel in I1 is 4.3 mm, in I2 is 5.3 mm. The worn crown surfaces have the form close to an isosceles triangle. A small "islet" representing the exposed pulp cavity is situated in the center of the triangle. The I3 is much larger than the median incisors, about doubled in width, although its wear surface is only slightly larger than those of the median ones. The mesial half of the I3 crown is probably only as high as those of the median incisors, while its distal half is much higher so that the base line of the enamel ascends steeply towards the distal end of the tooth. A distal carina accompanied by a medial groove is clearly shown. A tiny patch worn by the lower canine can be detected at the base of the distal carina. Neither cingulum nor other tubercles are present.

The canine is laterally compressed with the basal portion of the labial surface more

flattened. Seen from the lateral side, the anterior border of the crown is almost straight and vertical, while the posterior border is concave, and stretches antero-inferiorly in general direction (see Fig. 2). The basal line of the crown is slightly wavy, with a narrower anterior depression on lingual side and a wider one in the anterior half on the labial side. The antero-lingual carina is blunt, takes its origin slightly anterior to the antero-lingual depression, stretching slightly backward towards the canine tip. The posterior carina is more prominent and sharp, with imperceptibly fine serration and accompanied lingually by a shallow groove. The root is robust, with its cross-section near the base of the crown more elongated than that of the crown base (see Table 3). Anterior to the antero-lingual carina a stripe of worn facet can be seen, and on the top of the crown a tiny worn facet can also be seen.

The three anterior premolars are similarly constructed, all slightly worn. All are small, longer than wide and high, button-shaped, each with a median carina throughout the tooth, but without anterior and posterior cusplets. The P1 is the largest and longest, appressed on the postero-lingual corner of the canine root. It is single-rooted. The P2 is the smallest premolar, seemingly single-rooted seen at the alveolar border and within the right maxilla (Fig. 7B), but might be double-rooted within the left maxilla (in CT slide 5004, not shown in Fig. 7). The P2 is diagonally positioned with its anterior end turning lingually. The P3 is the tallest among the three, but about equally long as the P2, and double-rooted (Fig. 7B). The paracone of the P4 is the tallest cone of all the cheek teeth. It is conic in shape, but rather laterally compressed, with a convex buccal surface. The metastyle is about 2/3 the length and height of the paracone, judged on the less worn left P4. On buccal side the metastyle is separated from the paracone by a deep carnassial notch. The wear facets on the posterior half of the lingual sides of the paracone and the entire metastyle face postero-lingually in almost vertical plane so that a real carnassial blade is formed. Unfortunately, the protocones of both P4's are damaged during preparation when the lower teeth were detached from the upper ones. The protocone is small and apparently situated opposite, or slightly anterior to the carnassial notch (Fig. 7B). The tooth is almost entirely encircled by a cingulum. The P4 is superficially double-rooted, with its lingual and posterior buccal roots coalesced, leaving a groove between them on postero-lingual side, but internally they remain tri-rooted (Fig. 7B). All the four premolars are closely situated, leaving hardly discernible diastema between them.

The left M1 is better preserved than the right one. The M1 forms a rounded square in occlusal view, with its lingual borders rounded. Its buccal border is weakly convex, with a shallow central notch. The anterior border is slightly concave, while the posterior border is slightly convex. The paracone and metacone are about equally high, taking the shape of a trihedral pyramid. The buccal side of the pyramid is convex, while the lingual side is vaguely divided by a blunt ridge into two roughly flat surfaces of about equal size. The protocone forms a low, slightly buccally concave ridge, attenuating towards the anterior end of the paracone. The metaconule is prominent, slightly higher than the protocone, situated more lingual to the posterior end of the protocone and sending a ridge posteriorly. The crest linking the metaconule

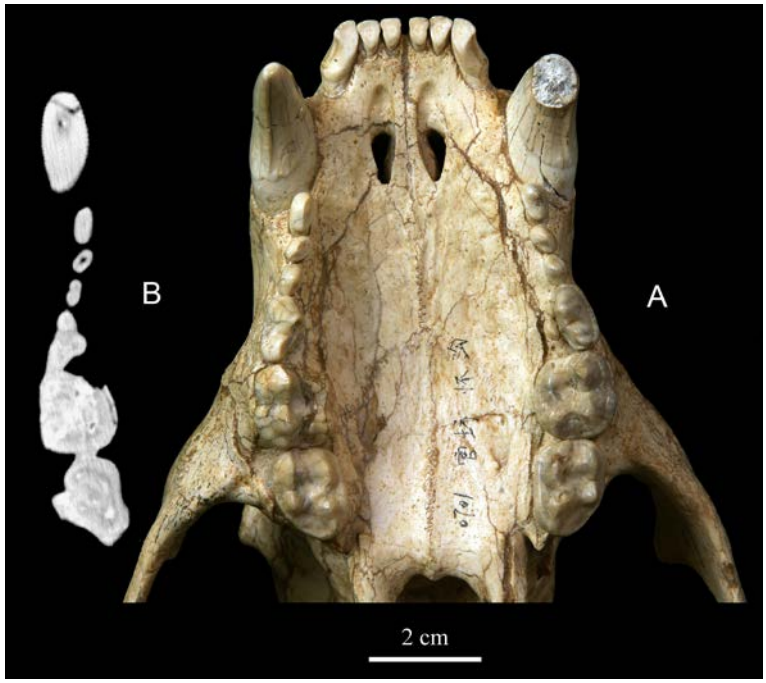

Fig. 7 *Ursavus tedfordi* sp. nov., HMV 1453 (holotype), ventral view
A. upper dentition; B. horizontal CT scanned slice 5014, taken slightly above the alveolar border of right maxillary, showing the roots of the premolars

with the metacone is vaguely formed, V-shaped seen from anterior or posterior side, hardly bordering the trigon basin posteriorly. No parastyle can be distinguished, while a tiny metastyle is represented by the posterior end of the buccal cingulum. A prominent cingulum runs through the entire buccal side, forming a band at about half the crown height. The lingual cingulum extends from above the crown base of the antero-lingual corner obliquely toward the metaconule, ended at the top of that cusp. The anterior cingulum is hardly noticeable, while the posterior cingulum is lacking. The M2 is only slightly longer, but evidently narrower, than the M1, with a short talon. All the occlusal elements of the M2 are similar to those of M1 in general morphology. The paracone and metacone are markedly lower and the metacone being the smallest in size, without a posterior carina. The protocone ridge is more prominent, with its anterior end reaching the middle of the anterior border of the tooth, and a hardly discernible posterior line leading apparently toward the metacone. The metaconule is wider separated from the protocone, without the buccal crest connecting the metacone as in M1. The posterior carina of the metaconule extends postro-lingually, then merging with the posterior rim of the talon basin. The talon is smaller than the trigon, with its postero-buccal border forming an angle of 140° with the buccal border of the para- and meta-cone. The talon surface is smooth, weakly deflected postero-buccally. The buccal cingulum is slightly weaker, while the lingual cingulum is continuous from the anterior end of the protocone to the posterior end of the metaconule, forming a shelf at the groove separating the protocone from the metaconule.

Table 3 Measurements of anterior upper teeth of some primitive ursid taxa (mm)

	Ursavus			*Ailurarctos*
	tedfordi	*brevirhinus*	*ehrenbergi*	*lufengensis*
	Huaigou HMV 1453	Hofmann,1892	Euboa Thenius, 1947	Qiu & Qi.,1989
1. H of C crown	30	12		
2. L of C crown	18.5	11		
3. W of C crown	12.1	7		
3/2 (%)	65.4	63.6		
4. L of C root	20	12		
5. P1 L	7.4	5.5	6.3	
6. P1 W	4.5	3	4.2	
7. P2 L	5.5	5.8	5	8.6
8. P2 W	3.6	3		5.2
9. P3 L	6.2	6.8		12.2
10. P3 W	4	3.2		7.4

Note : L. length; W. width; H. height.

Lower dentition (Fig. 8; Table 5) The lower incisors are less strongly worn than their upper counterparts. The wearing is effected only on the tops of the incisors. The wear facet on i1 is square, on i2 is rectangular, wider than long. On labial side the crowns of both i1 and i2 are about equally high, while on ligual side the crown of the i2 is about doubled wide and high than i1. Furthermore, the lingual side of the i2 is provided with a prominent central ridge flanked by lateral grooves. The i3 has a distal cusplet. Its crown wear facet is triangular in form, and its lingual surface is fin-shaped. The lower canine is similar to the upper one, but stronger curved in lateral view. Its mesio-lingual and distal carinas are about equally strong, but both are less developed than in the upper canine. A blunt third carina is developed in the upper half on the labial surface, and a wear facet resulted from the upper canine can be seen lingual to the third carina (see Fig. 6 wf).

The mesio-distal widths × labio-lingual lengths of the lower incisors are: i1: 2.5 × 5; i2: 3.6 × 7.4; i3: 6.7 × 7. Height × length × width of the c crown: 28.7 × 17.4 × 11.8. Length × width of the c root: 19 × 12 (all in mm).

The lower premolars are basically constructed as their upper counterparts. The p1 is the largest, button-shaped, and single-rooted. The p2 and p3 are about equally sized, seemingly single-rooted seen from the lingual side at the alveolar border, but with groove on buccal side. Therefore, they may be double-rooted within their alveoli. The p4 is much larger than the anterior three premolars, and definitely double-rooted. It bears a tiny anterior cusplet formed by the anterior bulge of the anterior carina, while the posterior cusplet is slightly better differentiated. The lingual cingulum is faintly shown at the anterior and posterior corners. No postero-lingual carina or cusplet is developed. There are diastemata between the premolars, that between p2 and p3 being the longest, ~2.5 mm.

The m1 is the longest of the lower cheek teeth. It is wider across the talonid than trigonid, and the base of the enamel is conspicuously flexed dorsally between the two roots (see Fig. 6 df). The trigonid is much higher than the talonid, The height of the trigonid (measured from the

Table 4 Measurements and comparison of upper teeth of *Ursavus* and some other ancestral ursid taxa (mm)

	Ballusia		*Ursavus*					*Kretzoiarctos*	*Agriarctos*	*Ailurarctos*
	elmensis	*orientalis*	*tedfordi* Huaigou HMV 1453	*brevirhinus*	*intermedius*	*primaevus*	*ehrenbergi* Euboa	*beatrix*	*depereti*	*lufengensis*
	Dehm, 1950	Qiu et al., 1985		Hofmann, 1892	Heizmann, 1973	Gaillard, 1899	Thenius, 1947	Abella et al., 2011	Crusafont-Pairo & Kurtén, 1976	Qiu & Qi, 1989
1. L of C-M2			80.7	66.5						
2. L of P1-M2			64	53.7						
3. L of P4-M2			45.2	36			49.2			
4. P4 L	{5}9.4−10.7[10.3]	8.5	12.5	12	11.4	13	14.5	18.5	19.7, 21.3	15.5
5. P4 W	{5}6.3−7.3[6.9]	5.3	~8.2	8	8	8	9.5	13	13.1, 14.5	11.3
5/4 (%)	[67]	62	65.6	66.7	72.7	62	65.5	70	66.5, 68	73
6. M1 L	{16}[12.2]	9.9	15.8	12	12.5	13	16.5	17.2	18.9, 19.9	17.3
7. M1 W	{16}[8.5]	9.2	15.2	10.2	11.2	12	14.8	15.4	16.7, 17.2	15.4
7/6 (%)	{16}[70]	93	96.2	85	90	92	89.7	85	88, 86.4	89
8. M2 L	{5}[12.2]	9	17	11.5	13.3	17	19.5		23.4, 21.3	19.8, 17.6
9. M2 W	{5}[8.3]	8.1	12.8	10	9.9	13	14.3		16.2, 15.8	14.9, 14.2
9/8 (%)	{5}[68]	90	75.3	87	74.4	76	73.3		69.2, 74.2	75.3, 80.7
6/4 (%)	[118]	116	126.4	100	107	100	113.8	92.9	96, 93.4	111.6
8/4 (%)	[118]	106	136	96	117	131	134.5		119, 100	127.7, 113.5
8/6 (%)	[100]	90	107.6	96	106	131	118.2		118.8, 107	114.5, 101.7

Note : Number of specimens in{ }, average in [ ] calculated by the present authors; L. length; W. width.

Table 5 Measurements and comparison of lower teeth of *Ursavus* and some other ancestral ursid taxa (mm)

	Ballusia			*Ursavus*				*Kretzoiarctos*	*Agriarctos*	*Ailurarctos*
	elmensis		*orientalis*	*tedfordi*	*brevirhinus*	*intermedius*	*primaevus*	*beatrix*	*depereti*	*lufengensis*
	Holotype Stehlin, 1917	Dehm, 1950	Holotype Qiu et al., 1985	Huaigou	Holotype Hofmann, 1887	Heizmann, 1973	Crusafont-Pairo & Kurtén, 1976	Abella et al., 2012	Holotype Schlosser, 1902	Qiu & Qi, 1989
1. L of p1		{3}(1.9−2.2)	3.5	8.2	6	{1}(5)				
2. W of p1				5.5	3					
3. L of p2		{3}(5.3−6.2)	5	6.2	6	{1} (4.3)		7.7		
4. W of p2				4.1	3			4.8		
5. L of p3	6.5	{3}(5.8−6.1)	5.3	5.2	6.5, 7	{1} (5.4)		8.9		
6. W of p3			2.2	4	3.2, 4			5.3		
7. L of p4	8.5	{3} 7.9−8.5	6.4	9.8	7.5, 8	{1} (7.2)	9.4; 9.6			13.9
8. W of p4			2.8	5.5	3.8, 4.5		4.9; 5.1	6.4		7.9
9. L of m1	14	13.7, 14	12.2	19.5	16, 18	14.9	{5} 19.2-21.2 [20.2]	22.6	23.5*	20.7**
10. L of m1 trigonid on lingual side	8*			12.5					17*	13.6**
11. W of m1 trigonid	5.3*			7.9					11*	9.4**
11/9 (%)	37.9			40.5					46.8	45.4
12. W of m1 talonid	6		7.2	8.9	?, 8.3*	8.2	{5} 9.5-10.4 [10]	10.8	12.6*	11**
12/9 (%)	42.9		59	45.6	46.1	55	{5} 44.8-52.6 [49.8]	47.8	53.6	53.1
13. H of m1 trigonid	6.4*			10.7	8				12*	11**
14. H of m1 talonid	4.1*			7					10*	7**
15. L of m2	10.2	10, 10.1	9.6	16	11.8, 12	12.4	{5} 14.2-15.9 [14.9]	17.7	17.3*	17.2
15/9 (%)	72.9		78.7	80.1	73.8, 66.7	83.2	{4} 71.8-75 [73.8]	78.3	73.6	83.1
16. W of m2 trigonid	6.4		6.1	10.5	7, 8	~7.5	{4} 9.2-9.9 [9.6]	11.3	11.6*	12.9
16/15 (%)	62.7			65.6	59.3, 66.7	~60.5		63.8	67.1	75
17. W of m2 talonid	5.5			9.7			{4} 8.8-9.5 [9.2]		10.7*	
17/15 (%)	54			60.6			{4} 57.9-66.9 [62.1]		61.8	
18. L of m3		{3}(4.8−5.8)	5	10.5	6.8		9.7; 10.8			10.7
19. W of m3			4.7	8.9	6.2		8.5; 8.3	9.7		9.6

Note: Number of specimens in {}, average in [ ], and measurements based on alveolars in ( ); * measured on figures by the authors of the present paper; ** measured based on unpublished specimen; L. length; W. width; H. height.

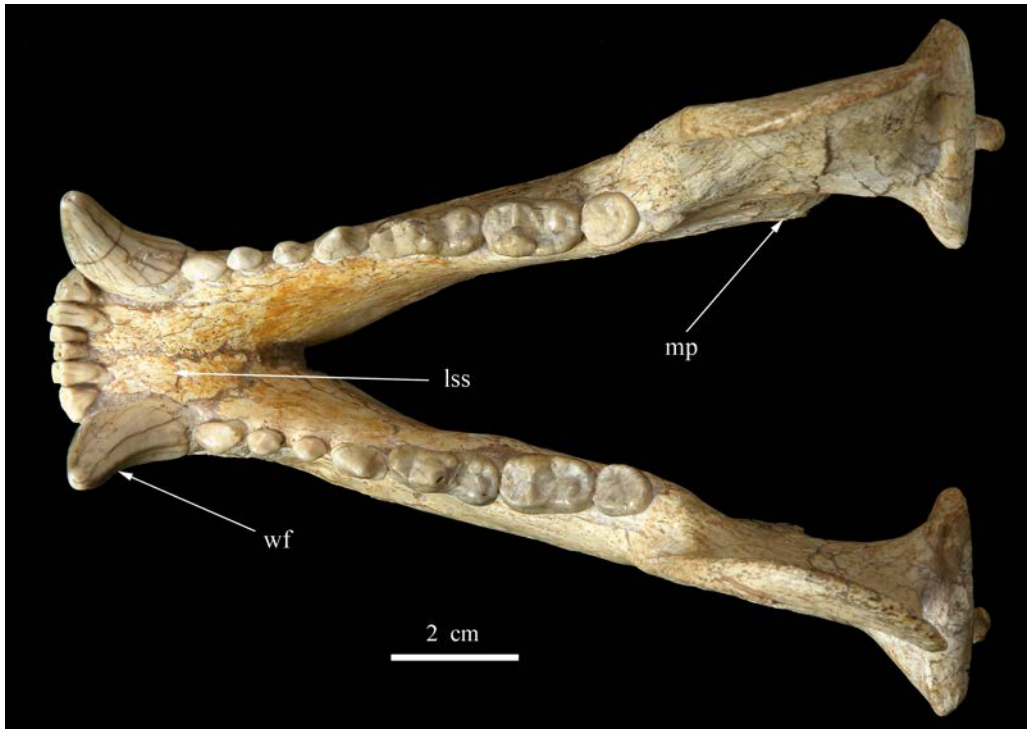

Fig. 8 *Ursavus tedfordi* sp. nov., HMV 1453 (holotype), mandible, crown view
Abbreviations: lss. lingual surface of symphysis; mp. marginal process; wf. wear facet caused by upper canine

lowest point of the base to the protoconid tip on buccal side) is approaching its length (measured from the anterior-most point of the paraconid to the valley separating the talonid from the trigonid on buccal side), and 1.5 times higher than that of the talonid (measured from the crown base to the hypoconid tip). The post-paracristid and the pre-protocrstid together form a V-shaped (~110º) carnassial blade seen from the sides. The shearing facet on the buccal side of the carnassial blade is almost vertical in position. On the right m1 the occlusion appears to be stronger, resulting in formation of a shearing strip on the top of the paraconid. The posterior side of the protoconid bears also a wear facet caused apparently by the M1 paracone. A post-lingual crest descends from the apex of the protoconid, connecting the metaconid at the latter's anterior end. The metaconid is very small, less than 1/2 of the paraconid in size, but situated high, only slightly lower than the tip of the paraconid. A faint posterior cristid descends from the tip of the metaconid downward to the lingual side of the bottom of the transverse valley separating the trignid from the talonid. There is no pre-metaconid at all. The hypoconid is robust, occupies about 2/3 of the talonid width, therefore the talonid is not basin shaped, but forming a longitudinal groove in the lingual half. Both the pre- and post-hypocristid are faintly shown, descending from the buccal side of the hypoconid. The pre-hypocristid extends to the transverse valley separating the talonid from the trigonid, while the post-hypocristid merges with the posterior rim of the talonid. The entoconid is doubled (the posterior one is often called

entoconulid). The twine cusps of the entoconid are of about equally size, widely separated from the metaconid by the transverse valley. They are slightly higher than the hypoconid so that they are visible from the buccal side. There is only a short, weak cingulum visible on the buccal side of the hypoconid (see Fig. 6 bc). The m2 is rectangular with rounded angles. It is shorter, but wider, than the m1. The trigonid basin is comparatively large, about 1/2 as long as the m2. The paraconid and metaconid form a roughly mirror-pair of low trihedrals. The metaconid is the highest cusp of the tooth so that it can be seen from the buccal side. A cusplet is differentiated from the pre-protocristid at the antero-buccal corner of the tooth, while the pre-metacristid is represented by two such cusplets. The V-shaped crest linking the protoconid and metaconid separates the trigonid from the talonid clearly. The post-protocristid forks in its posterior half: the buccal one is connected with the hypoconid, whereas the lingual one extends towards the centre of the talonid basin. The hypoconid and entoconid are generally similar to those of the m1, but the doubled entoconid seems larger and more crest-like. The buccal cingulum can hardly be seen. The m3 is oval in outline, with its anterior border straight and the posterior end slightly pointed. The occlusal surface is rather flat, with only the protoconid still recognizable. The protoconid is but a miniature of the m2, with its lingual crest extending postero-lingually.

3 Comparison and discussion

3.1 History of investigation of the ancestral forms of the living bears

The genus *Ursavus* had occupied a central position in study of the early ancestral forms of the livng bears prior to the 1940's. Almost every student studying ursid carnivores had considered *Ursavus* the unique ancestor of living bears since the end of the 19th century. The genus *Ursavus* was established by Schlosser in 1899, based on three forms: *Cephalogale brevirhinus* Hoffmann, 1887, *Hyaenarctos minitus* Schlosser, 1888 (published by Koken, but considered synonymous with *U. brevirhinus* by Schlosser in 1899) and *Ursus primaevus* Gaillard, 1899. Based mainly on the material of *U. brevirhinus* then available (two incomplete hemimandibles, one maxillary with upper dentition and some isolated teeth) from 3 localities (Steieregg and Voitsberg, Austria; and Kieferstadtel in Oppeln, now Poland), Schlosser (1899:101–102) characterized his new genus in rather general terms.

From the context of Schlosser's description the following can be viewed as more diagnostic for his new genus, in comparison with the living bears: size is small, about wolf-sized (Hünerhund). Canines are more laterally compressed, with clear anterior and posterior keels. Premolars are always four in number, separated by short diastemata. Except P4, all premolars are simple, without secondary cusplets. The second and third premolars are double-rooted. P4 metastyle is blade-shaped, its protocone considerably far posteriorly shifted [sic, should be corrected as anteriorly], with strong inner cingulum. The crown surfaces of molars are strongly wrinkled. Upper molars are rectangular, slightly longer than wide, each with two outer and two inner cusps, massive inner basal bulge and well developed external cingulum.

M2 with short talon. The m1 trigonid is much higher than its talonid, which is large, with strong, but low hypoconid and small entoconid. The m2 protoconid is low, but metaconid considerably strong, without paraconid. The m3 is knob-formed.

Later, with increasing finds of new materials from Early and Middle Miocene deposits, majority of which were, unfortunately, isolated teeth, *Ursavus* had gradually become a large heterogeneous genus. Up to now, in addition to the above 2 species, some 9 forms were established: *U. depereti* Schlosser, 1902, *U. elmensis* Stehlin, 1917, *U. intermedius* Koenigswald, 1925, *U. pawniensis* Frick, 1926, *U. primaevus* mut. *steinheimensis* Depéret & Llueca, 1928 (later described by Heizmann [1973] as *U.* cf. *intermedius*), *U. ehrenbergi* (Brunner, 1942, but described in detail by Thenius in 1947), *U. orientalis* Qiu, Yan & Jia, 1985, *U. sylvestris* Qiu & Qi, 1990, and *U. isorei* Ginsburg & Morales, 1998.

Opinions differed widely among paleontologists as to the reliability of referral of some of these species to the genus *Ursavus*. At least two species, *U. depereti* and *U. elmensis*, were formally excluded from the genus *Ursavus* (Kretzoi, 1942; Ginsburg and Morales, 1998). While establishing a new genus, *Agriarctos*, based on some isolated lower cheek teeth from Rózsaszentmárton and Hatvan (MN 13), Hungary, Kretzoi (1942) transferred the type specimen (m1 and m2 from Melchigin) of *Ursavus depereti* to his new genus *Agriarctos*, and tended to associate it with his smaller species, *Agriarctos vighi*. Based mainly on the diagnostic characters of the m1, i.e., the tooth being short and wide, with strong, anteriorly shifted metaconid, thus forming a rather closed trigonid, *Agriarctos* was considered by Kretzoi an intermediate form between *Ursavus* and the *Agriotherium-Indarctos* lineage. On the other hand, the right mandibular fragment with m1 and m2 from Luzinay, France, which was referred by Depéret and Llueca (1928) to *U. depereti* as well, was considered by Kretzoi as an unnamed member of *Ursavus*, but not *Agriarctos depereti.*

Without paying attention to Kretzoi's *Agriarctos* paper, Viret continued to use the name *U. depereti*, and referred a maxillary with P4 and M1, and an M2 from Soblay (MN 10), France, to it in 1949. In 1979, Thenius reallocated the Soblay material to the genus *Agriarctos*, but designated it as *Agriarctos* sp. In 1998, Ginsburg and Morales accepted Kretzoi's point of view, but referred the Soblay material to *Agriarctos* cf. *gaali* (type species of the genus). As the case with Viret, Qi also referred a few isolated teeth from the famous *Lufengpithecus* site in Yunnan, China, to *Ursavus depereti* in 1984. Later in 1989 this material was used by Qiu and Qi to establish a new genus and species, *Ailurarctos lufengensis*, belonging to the giant panda lineage.

Ginsburg and Morales (1998) also established a new genus, *Ballusia*, based on *Ursavus elmensis*. Diagnostic features of this new genus can be summarized (based on Ginsburg and Morales, 1998:105) as: size generally smaller than *Ursavus*; the lingual crest (formed by protocone and metaconule) of upper molars widely separated from the buccal cusps (paracone and metacone), lingual cingulum wider and more curved; M2 clearly elliptical, with short but wider talon; the m1 resembling those of *Hemicyon* and *Plithocyon* in having higher trigonid.

In addition to the type species (*B. elmensis*), another form, *Hemicyon hareni* Ginsburg, 1989, from Les Beilleaux and Faluns d'Anjon (MN 3), France, was also assigned to this genus, i. e., *Ballusia hareni*. On the other hand, Ginsburg and Morales (1998:109) suggested that *U. orientalis* might be close to the root of this lineage so that a new genus should be erected for it, but Qiu and Qiu (2013:145) temporarily transferred it to the genus *Ballusia*.

Just recently, Abella et al. (2012) created a new genus, *Kretzoiarctos*, based on a combination of a partially preserved right hemimandible from Vallès-Penedès with a left P4 and an M1 discovered from Nombrevilla 2, first identified as a new species of *Agriarctos* (*A. beatrix*) by Abella, Montoya and Morales in 2011. Based on cladistic analysis, Abella and colleagues concluded that *Kretzoiarctos beatrix* was the oldest recorded member of the giant panda lineage.

Employing Hennig's argumentation, Ginsburg and Morales (1998) came to the conclusion that the earliest member of the Ursinae is *Ballusia*, which gave rise to the *Ursavus-Ursus* lineage, while *Agriarctos* gave rise successively to *Agriotherium* and *Indarctos*, and finally *Ailurarctos* and *Ailuropoda* formed the pair of sister taxa. As thus defined, the primitive members of the Ursidae include: *Ballusia* (3 species: *B. elmensis*, *B. hareni* and *B. orientalis*), *Ursavus* (8 species: from Europe: *U. isorei*, *U. brevirhinus*, *U. intermedius*, *U. primaevus*, and *U. ehrenbergi*; from China: *U. sylvestris* and *U. tedfordi*; from North America: *U. pawnienesis*), *Agriarctos* (3 species: *A. depereti*, *A. gaali* and *A. vighi*), *Ailurarctos lufengensis* and *Kretzoiarctos beatrix*, altogether 5 genera and 16 species.

3.2 Comparison of *U. tedfordi* with the other early members of Ursidae

The tooth morphology of the Huaigou specimen (HMV 1453) is in overall conformity with the typical *Ursavus* (sensu stricto) as above described.

Specifically, HMV 1453 clearly differs from those of the Eurasian Early and Middle Miocene species, *Ballusia elmensis*, *B. hareni*, *B. orientalis*, *Ursavus isorei*, *U. brevirhinus*, and *U. intermedius*, in size and tooth morphology. All the above listed species are much smaller in overall size (see Tables 1–5) and more primitive in characters, such as the short molars relative to premolars (P1–P4 longer than M1+M2, p1–p4 longer than m1+m2), the strong development of lingual cingulum and wrinkles on crown surface of the upper molars, the 1st premolars being smaller than the other pre-carnassial premolars, the protocone of P4 more anteriorly located, and the m3 being small and oval in shape (especially in *Ballusia*).

The late Middle Miocene European *Ursavus primaevus* is closest to *U. tedfordi* in size (see Tables 4, 5). However, they differ from each other by different evolutionary levels in lengthening of the molars relative to premolars. In *U. primaevus* the M1 has the same length as the P4, while in *U. tedfordi* the M1 is definitely longer than the P4 (see Table 4). The same holds true in lower teeth. In the first species the lengthening of the m2 relative to the m1 is evidently less than in the second species (see Table 5) as well. Morphologically, the first species differs from the second one by retaining a longer and shelf-like lingual cingulum on

M1 and clear buccal cingulum on m1.

In size and general morphology the Late Miocene *Ursavus ehrenbergi* is most closely similar to the new species from Huaigou. However, it differs from the latter by a number of characters. 1) Its size is larger in general (see Tables 1, 4). 2) Its muzzle is wider (palatal width at C is 66.5 mm) and higher (height around P3 is 53.8 mm), while these measurements in *U. tedfordi* are 61 and 40 mm respectively (see Table 1). 3) The margin of nasal aperture in *U. ehrenbergi* is more vertical, forming an angle of 20° with the vertical axis of the skull, but about 30° in *U. tedfordi.* 4) Its palate is broad, with the distance between the lingual sides of the M2's is 49.6 mm, while in *U. tedfordi* it is much narrower, only 34.5 mm (see Table 1). 5) Its infraorbital foramen is located above the anterior rim of the posterior root of the P4, while in *U. tedfordi* it is above the boundary between the P4 and M1. 6) Its P2 and P3 are both double-rooted, while in the latter the P2 is in initial stage of becoming single-rooted, and the P3 is only internally double-rooted. 7) Its M1 is longer than wide but shorter relative to its P4 (M1L/P4L% = 113.8), while in *U. tedfordi* the M1 is almost quadrate in form but longer relative to its P4 (M1L/P4L% = 126.4). 8) Its M2 is about equally wide as the M1, while in *U. tedfordi* the M2 is much narrower than M1 (see Table 4).

Although the specimens of the above listed European species suitable for the purpose of comparison are very limited, it seems safe to say that the Huaigou specimen cannot be ascribed to any of them. The Huaigou specimen warrants a separate species status, here named as *Ursavus tedfordi*.

3.3 Comparason of the *Ursavus tedfordi* skull with those of living bears

So far no complete skull in association with its mandible has ever been described for any of the genera *Ballusia*, *Ursavus*, *Kretzoiarctos*, *Agriarctos* and *Ailurarctos.* The best material so far known is an anterior half of skull of *U. ehrenbergi* (Thenius, 1947) and two fragmentary hemimandibles of *U. brevirhinus* described by Hofmann (1887). This blank is now filled by the Huaigou specimen. Being one of the latest occurred (~8 Ma) and highly advanced member of the early ancestral ursids, the Huiagou skull may be quite different from the majority of the species in Early-Middle Miocene and early Late Miocene in possessing more advanced characters leading to the living bears. Therefore, it is highly important to ascertain the similarities and differences between *Ursavus tedfordi* and the living bears in skull morphology.

The notable common characters between *U. tedfordi* and the living ursine bears (excluding the giant panda) are: 1) The alisphenoid canal is present, with its posterior opening situated close to the *foramen ovale* and its anterior opening being confluent with the *foramen rotundum.* It is interesting to note that in the Hemicyoninae the alispenoid canal is present as an individual canal, separated from *foramen ovale*, while in the *Indarctos-Agriotherium* and *Ailuropoda* group this canal is absent. 2) The anterior pit "excavated in the basisphenoid," "wherein the [carotid] artery makes a 180 degree turn caudal to form the loop within the inferior petrosal sinus" (Hunt, 1977:839), a diagnostic character of the living ursines is present

in the Huaigou skull (vide supra), but so far not reported in the other above mentioned groups. 3) The posteiror border of the hard palate (the anterior border of the medial pterygoid fossa) extends posteriorly beyond the posterior border of M2 in both Huaigou and living bears, but in the above listed other groups the posterior border of the palate is aligned with, or anterior to, the posterior border of the M2. 4) The P4 is strongly reduced, much shorter than M1, with its protocone being small and simple, without parastyle, and tending to be double-rooted, while in other groups the P4 is well developed, equal to, or surpassing M1 in length, with large or duplicated protocone, and always tri-rooted.

The Huaigou skull distinguishes from the living ursine bears in the following points: 1) The posterior half of the frontal bones is strongly vaulted, forming the highest point of the cranium, which is much higher than the postorbital processes and situated much far posterior to those processes. 2) The sagittal crest is very high, plate-like, with its posterior end overhanging the nuchal surface far posteriorly. 3) The orbit is rounded in form, without its postero-superior corner angled by the robust postorbital process of the frontal bone. 4) The posterior border of the hard palate is much less posteriorly shifted, with the length of the part posterior to the M2 less than 1+1/2 P4 length (see Table 1). 5) In the infratemporal fossa no separate sphenopalatine and pterygopalatine foramen are formed, instead they form a single commonly confluent foramen. 6) The zygomatic bone extends more posteriorly, with its posterior end lying beyond the anterior margin of the condyloid fossa. 7) The medial edge of the articular fovea does not stepwise descend down from the *foramen ovale*. 8) The ventral surface of the auditory bulla is not flat, but slopes ventrally toward the medial direction. Before reaching the lateral crest of the basiocciptal bone, a curved crest is formed, extending from the post-medial corner to the 2/3 length of the bulla. The crest is separated from the lateral crest of the basioccipital bone by a shallow groove formed by the entotympanic bone. 9) The small pit situated anteromedial to the bulla, where the "ursid loop" of the internal carotid artery is located, is present, but very short. 10) The mandible has a keeled mental process, situated below the middle of the lower canine. 11) The lower border of the horizontal ramus under the toothrow is almost straight, nearly parallel with the alveolar border. The labial side of the symphysis being subvertical, forming a 70° angle with the mandibular lower border. 12) On medial side the anterior border of the coronal process ascends from the anterior end of the m3 so that the posterior part of the m3 is markedly tilted upward, and the lingual border of the m3 is not situated lingual to the medial border of the coronal process.

Taken as a whole, there is no doubt that *Ursavus tedfordi* is the latest and the most advanced among known ancestral forms of the living ursine bears. However, in view of the precocious appearance of some features not seen in the living ursine bears, as above listed, *Ursavus tedfordi* might well be an aberrant form, being one of the latest sister taxa of the clade consisting of the living ursine bears.

3.4 Cladistic analysis of the Miocene ancestral members of the Ursidae

The principal aim of the present paper is to find the ancestral forms of the living bears. We intentionally exclude the extinct side branches of *Agriotherium* and *Indarctos* from the present analysis. One of the reasons for doing so is the lack of good skull material of *Agriotherium* (but an article on a complete *Agriotherium* skull in association with its mandible is being prepared for publication by the present authors). Owing to the fact that all the relevant forms, with the only exception of *U. tedfordi*, are represented by isolated teeth and poorly preserved mandibular material, we are compelled to construct a character matrix based on mandible and teeth only, to avoid producing excessive number of missing state codings. A more comprehensive cladistic analysis based on cranial and dental characters of majority of bear lineages, including the living bears, will be conducted after the other fossil bear skulls recently found from the Linxia Basin, especially the *Agriotherium* skull, have been published.

3.4.1 Taxa used in analysis

The taxa selected for the data matrix include only 11 more representative Eurasian species (vide infra). The specimens of the European taxa used are based on literature only, while for those of China (*Ballusia orientalis*, *Ursavus tedfordi* and *Ailurarctos lufengensis*) the original and some supplementaty specimens are used. For comparative purpose, specimens of living bears (*Helarctos malayanus*, *Selenarctos thibetanus*, *Ursus arctos* and *Ailuropoda melanoleuca*) in IVPP's Osteological Collection were extensively utilized as well.

The materials or literature of taxa used in the analysis are:

(1) *Cephalogale minor* (MP22–MP28 [32.5–24 Ma]) The genus *Cephalogale* is a highly heterogeneous genus. De Beaumont (1965) recognized about 8 or 9 species in Europe, ranging from Stampian to Aquitanian. De Bonis (1973) added another 2 Aquitanian species. As to its phylogentic position, opinions differ as well. Most European scholars believe that the early and primitive species of this genus could give rise to the true ursine genus *Ursavus*, while the late and advanced species should belong to Hemicyoninae or Hemicyonidae (Ginsburg and Morales, 1998; Ginsburg, 1999). Some other scholars, especially the American students, are inclined to put *Cephalogale* to Hemicyoninae as a whole (Hunt, 1998). At any rate, the comprehensive description of *Cephalogale minor* based on about 50 specimens from the Phosphorites du Quercy, France, by de Beaumont (1965), is the best candidate for the outgroup taxon in the cladistic analysis.

(2) *Ballusia elmensis* (MN3 [20.5–18 Ma]) The holotype of this species is a left hemimandible from Elmer Tunnel, Germany. Rather rich materials, mainly isolated cheek teeth and several fragments of mandibles found from Wintershof-West locality were described by Dehm in 1950. Ginsburg and Morales (1998) created a new genus for this species and added a new species to it, i.e. *Ballusia elmensis* and *B. hareni*. The latter species is represented only by a few isolated teeth from various localities of MN3a. Only the material of *B. elmensis* is employed in our cladistic analysis.

(3) *Ballusia orientalis* (Shanwangian, ~18 Ma) So far only the holotype specimen is known (Shanwang, Qiu et al., 1985).

(4) *Ursavus brevirhinus* (MN4–9 [18–11 Ma]) The specimens considered by the present authors as more reliably assigned to this species are mainly from Austria: Steieregg and Voitsberg (about MN5), and Göriach (MN6), described by Hoffmann (1887, 1892) and Thenius (1949a,b). The *Ursavus* specimens found in Kieferstädtel (Oppeln) referred by Wegner to *U. brevirhinus* apparently consist of two forms: small-sized and large-sized. Only the small-sized M1–M2 (Wegner, 1913: Pl. XII-16) are referable to *U. brevirhinus*. The Can Llobasteres material referred by Crusafont-Pairo and Kurtén (1976) to *U. brevirhinus* may represent the largest and the most derived variety of this species. Although the general crown morphology of the dentition of the Can Llobasteres material conforms to that of the above mentioned material, the single-rooted p3 and the presence of a large and well separated posterior accessory cusplet in p4 are quite unique for this species. All the above listed specimens are used in the present analysis.

(5) *U. intermedius* (MN6–7 [15–13 Ma]) The holotype of this species is the right m1 and m2 from Engelswies, described by Koenigswald in 1925. The specimens from Steinheim were referred to this species by Heizmann (1973) based on their size and the length proportion between the m1 and m2, which is proportionally longer. These are the only specimens used in the present analysis.

(6) *U. primaevus* (MN6–9 [15–11 Ma]) In addition to the holotype (P4–M2 and an m1 from La Grive-Saint-Alban), described by Gaillard in 1899, the specimens referred to this species by the present authors include all the large-sized specimens from Kieferstädtel (Oppeln), described by Wegner (1913) as belonging to *U. brevirhinus*, and those from La Grive-Saint-Alban described by Depéret and Llueca in 1928. The specimens from Can Ponsich (Spain) described by Crusafont-Pairo and Kurtén (1976) should also belong to this species, although slightly smaller in size.

(7) *U. ehrenbergi* (MN11 [8.7–8 Ma]) There is only one specimen, the holotype of the species, an anterior half of skull from Halmyropotamos (Greece) described by Thenius in 1947.

(8) *U. tedfordi* (late Bahean [~8 Ma]) The only specimen is the skull in association with its mandible described in this paper.

(9) *Kretzoiarctos beatrix* (MN8 [~11.6 Ma]) A P4 and an M1 from Nombrevilla 2 in the Calatayud-Daroca Basin were first described as a new species of *Agriarctos*, *A. beatrix* (Abella et al., 2011). A year later, based on a newly found left hemimandible from Abocador de Can Mata (ACM) in the Vallès-Penedès Basin, a new genus was erected by Abella et al. (2011, 2012). These are the only specimens of this species.

(10) *Agriarctos depereti* (MN9 [11–9.7 Ma]) The genus was established by Kretzoi (1942) based on a toothrow consisting of p3–m2 (p4 partly broken) from Hatvan (Hungary), and was described under the name *Agriarctos gaali*, which was also designated as the type species of his new genus *Agriarctos*. In the same paper Kretzoi transferred Schlosser's *U. depereti* to his new genus, thus renamed as *Agriarctos depereti.* The holotype of *A. depereti* is a left m1 and

m2 from Melchingen, Germany, first described by Schlosser in 1902 as *Ursavus depereti*. The other specimens referable to this species are the P4–M2 from Soblay, described by Viret in 1949, and those from Luzinay, a right hemimandibular fragment with m1 and m2, described by Depéret and Llueca in 1928. The type species, *A. gaali*, was also employed in the analysis in order to complement the lack of premolars in *A. depereti*.

(11) *Ailurarctos lufengensis* (late Baodean [6.8–6.3 Ma]) The material described by Qiu and Qi in 1989 was used. Some supplementary material recently found from the boxes containing the old specimens of carnivores of the Lufeng locality, including a complete right m1, was also employed in this analysis.

Ursavus hareni and *U. sylvestris* are not included in the present analysis because of their poor representation in fossils.

3.4.2 Character construction and character state coding (Appendices 1, 2)

Character construction is fundamental to cladistic analysis and evoked heated discussion in the last 20 years or so of the last century. In our cladistic analysis the following methods are practised in character construction: 1) The independence and discreteness are the two most important axiomatic principles in character construction. To abide by the independence principle, we prefer the "reductive coding" approach rather than "composite coding", as suggested by Wilkinson (1995), but not go to the extreme that binary absence/presence coding be finally reached as advocated by Pleijel (1995). In fact, linear and branching multistate transformation series as proposed by Wiley et al. (1991) are equally well applicable as binary coding, depending on circumstances. Only when covariation of characters can be positively assumed, "composite coding" can be allowed. For example, it is well known that the size reduction of premolars is covarying with the transformation from cone-shaped to button-shaped in ursid animals. The discretness is also important in character construction. In this regard, polymorphic taxa and polymorphic characters in taxa with high intraspecific variation are here avoided. For example, the enamel corrugation of the upper molars is generally a good indicator of phylogeny and clear polarity can be observed in some clades, e.g., *Ailuropoda* clade. However, this character was variously described by different authors regarding its development within some *Ursavus* species. Therefore, this character has not been used in our matrix. 2) Unique autapomorphic characters of terminal taxa are not necessarily all included in matrix. For example, the particularly long labial border of the M1 in *Ballusia orientalis* is such an autapomorphy. 3) Contrary to the common tendency to prefer the maximally connected (= unordered) characters in cladistic analysis, Slowinski (1993) strongly advocated that "multistate characters are treated as minimally connected (= ordered linear and branching transformation series of Wiley et al. [1991]) whenever reasonable." Slowinski's suggestion is adopted here in view of the fact that the evolutionary history (polarity and additive steps) of the multistate characters used in our matrix is fairly well known in ursid animals. Quoted from Page et al. (1992), Slowinski stressed again (1993:163) that: "useful information is lost when a correct 'ordering' is discarded." Accordingly, additive coding assumption is used here for most of the

linear multistate characters. 4) While dealing with the complex "branching transformation series," instead of using nonadditive binary coding or mixed coding as suggested by Wiley et al. (1991), we employ the "reductive coding" approach to partition composite character into smaller binary or linear transformation series according to the diverging evolutionany directions of the character (see characters 7–13 in Appendix 2). However, there is the possibility of producing "inapplicable" states alternatively in one of the two transformation series. To designate the "inapplicable" states by "?" in matrix would cause the mixture of two different conceptions (inapplicability and lacking) in coding. However, as Maddison (1993) has proved: "Coding inapplicable characters as missing data is safe in some circumstances," if "the only taxa with the character inapplicable are all members of a clade." Barriel and Tassy (1993) expressed similar notion by saying that "These unseen traits coded "?" will be optimized by parsimony analysis." and "The problem is solved if optimization is interpreted in terms of number of steps rather than states."

For character description see Appendix 2.

3.4.3 Cladisctic analysis

Cladistic analysis is performed using TNT ver. 1.1, March, 2009 – by Goloboff et al. (2008). The data matrix was generated using the TNT menu option Data/Edit on character by character basis. Since the data sets are very small (11 taxa and 37 characters), the Implicit Enumeration (IE, or branch-and-bound) tree-searching method under non-additive and additive assumptions was tried to obtain more exact solutions. Under non-additive condition the IE searching recovered 12 equally MPTs, all with a total length of 63 steps, CI = 0.810 and RI = 0.657. Under partially additive (13 out of 37) assumption 8 equally MPTs were recovered, with the same total length of 63 and the same CI (0.810), but a slightly higher RI (0.700), meaning more synapomorphies retained. This shows the searching under partially additive assumption is better than that under non-additive condition, and thus the partially additive assumption is chosen in searching algorithm. In order to get some idea about the robustness of the grouping in the obtained equally MPTs, standard bootstrapping (1000 replicates) was run.

Some of the obtained MPTs are shown in Fig. 9. Regarding the positions of *Ballusia elmensis* and *B. orientalis*, there are two options in the 8 MPTs: either *B. elmensis* occupies the most basal position in the ursid clade after its separation from *Cephalogale minor* (in tree 0, 1, 4 and 5), or *B. orientalis* is the basal one (in trees 2, 3, 6 and 7). Taking the apomorphic characters of *B orientalis* [reduced blade length in P4 (character 16 coding 2, henceforth simplified as 16-2) and the particularly wide m1 talonid (29-2) in trees 0, 1, 4 and 5, and the other two unrecorded characters (the particularly long labial border and the strong enamel rugosity in M1) into consideration, it is better to consider *B. orientalis* as an aberrant form derived from *B. elmensis*. In this case, only MPTs 0, 1, 4 and 5 (shown in Fig. 9) are in accordance with the above prerequisites and are to be further analyzed. A common feature in all the 4 adopted MPTs is the presence of a stable clade comprising of *Kretzoiarctos* (*Agriarctos*+*Ailurarctos*) or node 19 (node 8 + node 20 (9 + 10)), expressed in Wenn diagram.

It is a pity that the *Ursavus* clade is quite unstable in content and topology. In tree 0 (Fig. 9A) it is made up of only two species (*U. ehrenbergi* and *U. tedfordi*) and the other three species (*U. brevirhinus*, *U. intermedius* and *U. primaevus*) have succssively split off before the two-species *Ursavus* clade made its appearance. In tree 1 (Fig. 9B) two *Ursavus* subclades appeared: one was composed of *U. brevirhinus* and *U. intermedius* at node 14, while the other is composed of the other three species at node 17. In tree 4 (Fig. 9C) the *Ursavus* clade included four species excepting *U. brevirhinus*, which was the sister group of the two major clades: the *Kretzoiarctos* (*Agriarctos+Ailurarctos*) clade and the four-species *Ursavus* clade. Only tree 5 (Fig. 9D) shows that the earliest divergence (node 15) is the sister taxon of *Ballusia orientalis*. Our preference to tree 5 as the most reliable cladogram of the four equally MPTs is also based on morphological considerations. First of all, having been separated from *Ballusia*, *Kretzoiarctos*, *Agriarctos* and *Ailurarctos* at generic level, the genus *Ursavus* (sensu stricto) becomes much more homogenous than before. The morphological differences between the remaining *Ursavus* species (the above 5 species, plus the poorly represented *U. sylvestris* and *U. pawniensis*) are very small, either transitional, or gradual, and some times so mosaic in distribution that it is almost impossible to separate them further and regroup them into different genera based on presently available material. From the point of view of the nomenclatural stability, tree 5 is superior to the other trees as well. In tree 5 all the *Ursavus* species fall into a single clade, and can reasonably be grouped into the same genus. On the contrary, in the other trees either some of the *Ursavus* species are to be excluded from the *Ursavus* clade, or they form more than one clades. In such circumstances, it is not so easy to group all these species in the genus *Ursavus*. For example, in tree 4 *U. brevirhinus* is excluded from the clade comprising the other four species. In this case, cladistically we have to creat a new generic name for all the four *Ursavus* species. Since *U. brevirhinus* (type species of *Ursavus*) preoccupies the generic name *Ursavus*, taking such a procedure would be rather paradoxical in terms of currently practiced nomenclatural rules. On the other hand, tree 5 is superior to the other trees also for the *Kretzoiarctos*-(*Agriarctos+Ailurarctos*) clade, since at least one more apomorphic character (20-1-2) is added here than in tree 4 (Fig. 9E, F).

Specifically, in tree 5 (Fig. 9D) the sister group of *B. orientalis* is the largest clade (node 15) composed of the two major subclades of the Ursidae: the *Kretzoiarctos*-(*Agriarctos+Ailurarctos*) lineage and the *Ursavus* lineage. The node 15 has the following synapomorphies: high mandible (2-1), lingual cusps forming a three-cuspid crest in M1 (23-2), M2 relatively long and rectangular in form (25-1 and 26-2). The node 19 has the following synapomorphies: presence of parastyle (15-1-2) and doubled protocone of P4 (17-1-2) and low crown height of the m1 trigonid (27-2). The node 14 contains all the *Ursavus* species, united by the subquadrate crown form of the M1 (20-1-2).

The node 19 (*Kretzoiarctos* (*Agriarctos+Ailuractos*)) occurs in every MPT obtained during our searching under different conditions. Its robustness is further supported by bootstrapping algorithm under additive condition (Fig. 9G, grouping frequencies = 66 and 74).

On the other hand, the patterns of the *Ursavus* subclade are considerably variable: from being composed of only two species: *U. tedfordi* and *U. ehrenbergi* (in tree 0, 2), to three species, adding *U. primaevus* (tree 1, 3), to four species, adding *U. intermedius* (tree 4, 6) and finally to all five species, adding *U. brevirhinus* (tree 5, 7). This shows that the grouping of the *Ursavus* species are highly unstable. These groupings are also not supported by bootstrapping under both conditions (Fig. 9G). This is understandable as the fossil materials of these species are very poor and the characters are highly mosaic in distribution.

Although the living bears are excluded from our analysis, some clear hints emerge as to the origin of some of the living bears. Just recently, Abella and colleagues (2012) proclaimed that they found "the oldest recorded member of the giant panda lineage." Abella and colleagues' Ailuropodinae include two subclades: the *Indarctos* one and the ailuropod one, with *Ailuropoda* being the first split from the remaining members of the latter subclade (loc, cit, fig. 3). Our cladogram shows that *Kretzoiarctos* is a sister taxon to the other two genera (*Agriarctos* and *Ailuractos*). Since *Ailuractos* is certainly the earliest know ancestral taxon leading to *Ailuropoda* as clearly evidenced by the tooth morpholgy, *Kretzoiarctos* may not be directly ancestral to *Ailuropoda*. In fact, *K. beatrix* does't possess the key characters leading to *Ailuropoda*: the enlargement of the premolars, especially the anterior and posterior accessory cusps (see characters 7–13 in Appendix 2) and the short and V-shaped m1 trigonid (31-0). Unfortunately, these characters have not been recorded by Abella and colleagues in their character construction. On the other hand, these characters, together with the presence of small parastyle and doubled protocone of P4, can be found in *Indarctos* species. Thus, it is highly possible that *Kretzoiarctos* is the ancestral taxon of *Indarctos* clade, rather than that of *Ailuropoda*.

On the other hand, *Ursavus tedfordi* is evidently the most advanced in the *Ursavus* clade, characterized by possessing at least 5 apomorphic characters commonly shared with living bears (excluding *Ailuropoda*): straight lower mandibular border (0-1), confluent roots of premolars (14-1), P4 protocone situated around carnassial notch (18-3), P4 roots tending to be reduced to two (19-1), and strongly reduced lingual cingulum in M1 (24-2), indicating its closest relationships with the living ursines.

3.4.4 Classification

From the foregoing analysis and the resultant cladogram it follows that the early members of the Ursidae can be subdivided into three major subgroups.

The first and the stem group is composed of two earliest taxa of the Ursidae: *Ballusia elmensis*, *B. hareni* and *B. orientalis*. This group is characterized by the small body size and the M2 being oval in form and shorter than M1. *Ballusia orientalis* is a more advanced and aberrant form, and appeared later than the type species.

The major clade is the group comprising two subclades: the *Kretzoiarctos* and *Agriarctos+Ailurarctos* subclade and the *Ursavus* subclade, which should be the ancestral forms of the living bear (excluding *Ailuropoda*) lineage.

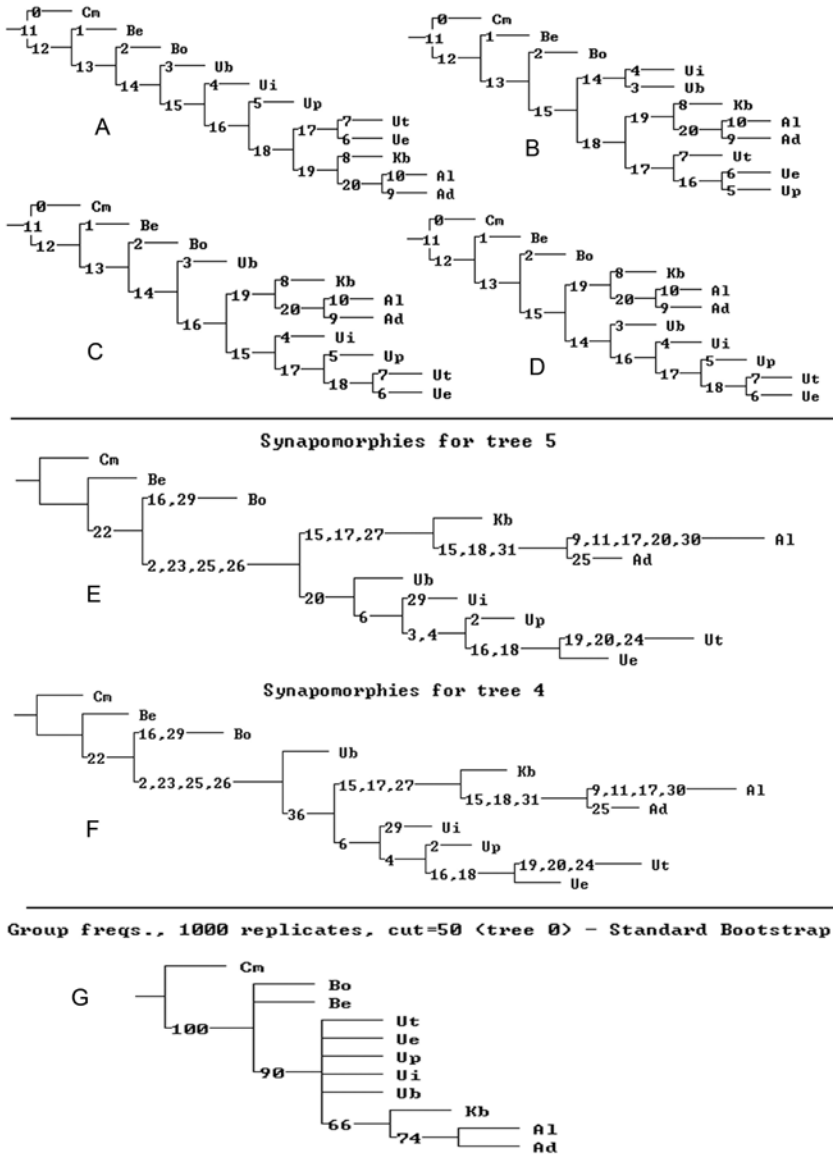

Fig. 9 Some of the MPTs obtained using IE searching in TNT, total length = 63 steps, CI = 0.81, RI = 0.7
Adopted MPTs: A. tree 0; B. tree 1; C. tree 4; D. tree 5; Synapomorphies: E. for tree 5; F. for tree 4 (for comparison); G. group frequencies obtained using standard bootstrapping
Abbreviations: Cm. *Cephalogale minor*; Be. *Ballusia elmensis*; Bo. *B. orientalis*; Ub. *Ursavus brevirhinus*; Ui. *U. intermedius*; Up. *U. primaevus*; Ue. *U. ehrenbergi*; Ut. *U. tedfordi*; Kb. *Kretzoiarctos beatrix*; Ad. *Agriarctos depereti*; Al. *Ailurarctos lufengensis*

A preliminary formal classification is proposed here as follows:

Ursidae

stem taxa

Ballusia, including *B. elmensis*, *B. hareni* and *B. orientalis*

Ursinae
Ursini
Ursavus
Ursus etc.
Tremarctini
Trmarctos etc.
Ailuropodinae
Indactini
Kretzoiarctos, including only *K. beatrix*
Indarctos
Agriotherium ?
Ailuropodini
Agriarctos, including *A. depereti*, *A. gaali* and *A. vighi*
Ailurarctos, including *A. lufengensis*
Ailuropoda

Acknowlegements The authors thank Mr. He Wen (director) and Mr. Chen Shanqin (vice-director) of the Hezheng Paleozoological Museum for their special kindness to the authors to prepare and study the beautiful *Ursavus* skull. Thanks are extended to all the technicians who helped to prepare the studied specimen (Mr. Li Fengchao), to take the photos (Mr. Gao Wei), and the CT scan slides (Mr. Zhao Shusen and Mr. Hou Yemao). In particular, we would like to thank Dr. Zhao Qi for his help and fruitful discussions with the authors on character construction problems and manipulation of the cladistic computer softwares. Special thanks are extended to Dr. Shi Qinqin, who drew the head reconstruction of *Ursavus tedfordi* (frontispiece). Finally, we would like to thank the two reviewers, Dr. Wang Xiaoming and Dr. Liu Jinyi, for their comments and valuable suggestions.

记甘肃广河晚中新世祖熊头骨化石

邱占祥 邓 涛 王伴月

(中国科学院古脊椎动物与古人类研究所，中国科学院脊椎动物演化与人类起源重点实验室 北京100044)

摘要：记述了一件与下颌咬合在一起的完整的祖熊头骨化石。化石发现于甘肃临夏州广河县槐沟村柳树组地层中上部，其层位与时代为新近纪灞河阶/期的晚期，距今约8 Ma。对比研究表明，该头骨与目前所有已知熊类祖先类型都不同，应为一新种，定名为*Ursavus tedfordi* (戴氏祖熊)。采用TNT软件包对11种祖先熊类和37个特征组成的数据进行不同条件(non-additive, additive等)下全搜索(Implicit Enumeration),并采用自引导法(bootstrapping)进行可信度评价。我们从基于部分特征加积(partially additive)条件下所得出8个最简约树中选取

树5作为最可信简约树。该树表明，熊科从渐新世—早中新世的豺熊类(hemicyonids)分出后产生了两类基干类型，*Ballusia elmensis*和*B. orientalis*。后者稍更进步，可能为一特异支。此后产生了两大次支：一支向印度熊(可能还有郊熊) +大熊猫演化；另一支则由中—晚中新世的祖熊(*Ursavus*)和此后由某类祖熊所产生的现生熊类(不包括大熊猫)组成。从现有的化石判断，新建戴氏祖熊是与现生熊类在形态上最为接近的祖先类型，但戴氏祖熊具有某些自近裔性状，可能为一早期旁支。

关键词：中国，晚中新世，祖熊，大熊猫

中图法分类号：Q915.874　　**文献标识码**：A　　**文章编号**：1000-3118(2014)03-0265-38

Appendix 1 Data matrix employed in the clasdistic analysis, including 11 taxa and 37 characters (for abbreviations see Fig. 9)

Cm	0	0	0	0	0	0	0	0	0	0	0	0	0	0	0	0	0	0	0	0	0	0	0	0	0	0	0	0	0	0	0	0	0	0	0	0	0
Be	0	0	0	0	0	0	1	0	1	1	?	1	?	1	?	0	0	1	0	1	0	1	1	1	0	1	1	0	1	1	1	1	0	0	1	1	1	1	0
Bo	0	?	0	0	?	?	0	1	1	?	1	?	1	?	0	0	2	0	1	0	1	1	1	1	1	0	1	1	1	2	0	0	1	0	1	1	0
Ub	0	0	1	0	0	1	0	1	1	?	1	?	1	?	0	0	1	0	1	0	2	1	1	2	1	1	2	1	1	1	0	0	1	1	1	1	0
Ui	?	?	1	0	0	?	1	?	?	?	?	?	?	?	1	0	1	0	1	?	2	1	1	2	1	1	2	1	1	2	0	0	1	1	1	1	?
Up	0	0	0	1	1	?	?	?	?	?	?	?	?	?	?	0	1	0	1	?	2	1	1	2	1	2	2	1	1	1	0	0	1	1	1	1	1
Ue	?	?	?	?	?	?	?	1	2	1	?	1	?	?	?	0	0	2	0	2	0	2	1	1	2	1	2	2	?	?	?	?	?	?	?	?	?	?
Ut	1	1	1	1	1	1	1	2	1	?	1	?	1	?	1	0	2	0	2	1	1	1	1	2	2	1	2	1	1	1	0	0	1	1	1	1	1
Kb	0	0	1	1	?	1	0	1	1	?	1	?	1	?	0	1	1	1	1	?	1	1	1	2	1	?	?	2	1	1	0	0	1	1	1	1	?
Ad	?	?	?	?	?	?	?	1	?	1	?	1	?	1	?	2	1	1	2	?	1	1	1	2	1	2	2	2	1	1	0	1	1	1	1	1	?
Al	?	?	?	?	?	?	?	1	?	2	?	?	1	0	2	1	2	2	0	2	1	1	2	1	1	2	2	1	1	1	1	1	1	1	1	1	1

Appendix 2 Character description (Altogether 37, 13 multistate characters bearing * treated as additive in analysis; a number of the characters used by Abella and colleagues in 2012, altogether 20 out of 82, are indicated in brackets following our character titles, but state coding may not be the same as Abella and colleagues proposed)

Mandible:

0. Lower border under the cheek teeth (Abella et al., 2012:11)**:** 0: tapering anteriorly, curved, or more or less straight; 1: straight and horizontal, extending posteriorly beyond the tooth row.

1. Symphysis (Abella et al., 2012:17)**:** 0: lower border slanting postero-inferiorly, confluent with lower mandibular border, forming an angle >135º; 1: more vertically, with angled chin, forming an angle < 135º.

2. Hight of horizontal ramus (Abella et al., 2012:16)**:** 0: height under m1-m2 / length of m1: < 1.4; 1: height under m1-m2 / length of m1: ~1.4−1.6.

3. Marginal (digastric) process (Abella et al., 2012:9)**:** 0: absent or hardly discernible;

1: well developed. For this character in *U. primaevus* see Crusafont-Pairo and Kurtén (1976: fig. 13).

4. Position of mental foramina: 0: posterior-most one situated anterior to p4; 1: under p4 or more posteriorly.

Dentition:

5. Canine height (Abella et al., 2012:1)**:** 0: crown height about twice as crown length at base, posterior margin weakly concave; 1: crown height about 3/2 as crown length at base, with strong posterior basal bulging.

6. P1(p1) enlargement: 0: small relative to other ante-carnassial premolars; 1: larger than other ante-carnassial

premolars.

***7. Reduction of P2−P3 and p2−p4 main cusps:** 0: large, laterally compressed cone-shaped, higher than long and wide; 1: shorter, more cone-shaped and slightly higher than wide; 2: much smaller, button-shaped, wider and/or longer than high.

8. Reduction of anterior accessory cusps of P2−P3 and p2−p4: 0: small or tiny, more or less differential from main cusp; 1: absent or tiny, undifferentiated.

***9. Enlargement of anterior accessory cusps of P2−P3 and p2−p4: 0:** small or tiny; 1: enlarged, well differentiated, much smaller than main cusps; 2: large and ridge-form, subequal to main cusps.

10. Reduction of posterior accessory cusps of P2−P3 and p2−p3: 0: small, more or less differentiated from main cusp; 1: absent or tiny, undifferentiated.

***11. Enlargement of posterior accessory cusps of P2−P3 and p2−p3:** 0: small; 1: enlarged, well differentiated, much smaller than main cusps; 2: large and crest-shaped, subequal to main cusps.

12. Reduction of posterior accessory cusps of p4: 0: large, well separated from main cusp, 1: small, hardly separated from main cusp.

13. Enlargement of posterior accessory cusp of p4: 0: large, cone-shaped, 1: long, crest-shaped.

14. Premolar roots of P2−P3 and p2−p3: 0: double-rooted; 1: roots of some or all of P2−P3 and p2−p3 incipiently coalesced, with pulp canals remaining separate internally.

***15. P4 parastyle (Abella et al., 2012:59):** 0. parastyle absent; 1: present, cone-shaped, much smaller than metastyle; 2: present, crest-shaped, subequal to metastyle.

***16. Reduction of P4 blade length (Abella et al., 2012:58):** 0: carnassial blade (including parastyle, if present) longer than M1; 1: about equally long or slightly shorter than M1; 2: markedly shorter than M1.

***17. P4 protocone form (Abella et al., 2012:61):** 0: single; 1: protocone with smaller anterior accessory cusplet; 2: doubled, consisting of about equally large pre-protocrista cone and protocone.

***18. P4 protocone position** (Abella et al., 2012:62)**:** 0: anterior to paraconid, extending antero-lingually; 1: opposite paracone, extending lingually; 2: posterior to paracone, with its posterior end reaching to the carnassial notch.

19. P4 roots: 0: tri-rooted; 1: incipient double-rooted, with posterior and lingual roots coalesced (internally separated).

***20. M1 crown shape** (Abella et al., 2012:66)**:** 0: trapezoid, wider than long, with lingual border much shorter than labial one; 1: subquadrate, with convex lingual border; 2: longer than wide, lingual side more or less straight.

21. Height of lingual cusps relative to labial cusps in M1: 0: lingual cusps about half high as labial cusps; 1: lingual cusps slightly lower than labial cusps.

22. Metacone-metaconule crest of M1 (Abella et al., 2012:67-68)**:** 0: absent; 1: present.

***23. Transformation of M1 lingual cusps:** 0: protocone V-shaped, metaconule situated postero-labial to protocone; 1: protocone and metaconule situated in the same longitudinal line, forming a very shallow W-shaped crest; 2: protocone, post-protocrista and metaconule forming a longitudinal crest.

***24. M1 lingual cingulum** (Abella et al., 2012:69)**:** 0: confluent with anterior cingulum, forming a strong curve and deep groove lingual to lingual cusps; 1: shelf or ridge-like, extending from anterior end of lingual side to metaconule apex; 2: strongly attenuated, may not be continuous.

***25. M2 length relative to M1** (Abella et al., 2012:70)**:** 0: much shorter than M1; 1: subequal to M1; 2: longer than

M1 (M2/M1 > 1.15).

***26. Crown form of M2** (Abella et al., 2012:71)**:** 0: trapezoid, wider than long; 1: oval; 2: subquadrate or trapezoidal, longer than wide.

***27. m1 trigonid height relative to talonid:** 0: trignid about twice as high as talonid; 1: trigonid about 1.5 times high as talonid; 2: trigonid only slightly higher than talonid.

28. m1 talonid length relative to trigonid, measured on labial side (Abella et al., 2012:38)**:** 0: talonid about half as long as trigonid; 1: talonid about 0.6−0.8 as long as trigonid.

2**9. m1 talonid width:** 0: talonid narrower than or subequal to trigonid in width; 1: talonid slightly wider than trigonid; 2: talonid evidently wider than trigonid.

30. Pre-hypocristid cusp in m1 (Abella et al., 2012:39)**:** 0: absent; 1: present.

31. m1 metaconid size and position (covariated, Abella et al., 2012:31)**:** 0: small, lower than paraconid, situated more posteriorly than lingually to protoconid; 1: large, subequal to paraconid in size, situated more diagonally to protoconid, thus forming a V-shaped trigonid.

32. m1 entoconid: 0: single cusplet or crested; 1: doubled.

33. m1 entoconid vs hypoconid: 0: entoconid lower than hypoconid; 1: entoconid slightly higher than hypoconid.

34. Posterior surface of trigonid of m1, viewed from lingual side (Abella et al., 2012:37)**:** 0: subvertical, more than 60º with horizontal line; 1: more or less diagonal, forming an angle around 45º with horizontal line.

35. m2 length relative to m1 (Abella et al., 2012:46)**:** 0: m2 approximately 1/2 as long as m1; 1: m2 about 0.7−0.8 as long as m1.

36. Size of m3 relative to m2 (Abella et al., 2012:54)**:** 0: length of m3 about 1/2 of m2; 1: about 2/3 of m2.

References

Abella J, Alba D M, Robles J M et al., 2012. *Kretzoiarctos* gen. nov., the oldest member of the giant panda clade. PLoS One, 7(11): 1−7

Abella J, Montoya P, Morales J, 2011. A new species of *Agriarctos* (Ailuropodinae, Ursidae, Carnivora) in the locality of Nombrevilla 2 (Zaragoza, España). Estud Geol, 67(2): 187−191

Barriel V, Tassy P, 1993. Characters, observations and steps: comment on Lipscomb's "Parsimony, homology and the analysis of multistate characters". Cladistics, 9: 223−232

Beaumont G de, 1965. Contribution à l'étude du genre *Cephalogale Jourdan* (Carnivora). Mém Suisse Paléont, 82: 1−34

Crusafont-Pairo M, Kurtén B, 1976. Bears and bear-dogs from the Vallesian of the Vallés-Penedès Basin, Spain. Acta Zool Fenn, 144: 1−29

Davis D D, 1964. The giant panda. Fieldiana: Zool Mem Chicago Nat Hist Mus, 3: 1−334

De Bonis L, 1973. Contribution a l'Étude des Mammifères de l'Aquitanien de l'Agenais, Rongeurs-Carnivores-Perissodactyles. Mém Mus Natl Hist Nat, Sér C, Sci Terre, 28: 1−192

Dehm R, 1950. Die Raubtiere aus dem Mittel-Miocän (Burdigarium) von Wintershof-West bei Eichstätt in Bayern. Abh Bayer Akad Wissensch Math-naturw Kl, Neue Folge, 58: 1−141

Deng T, Qiu Z X, Wang B Y et al., 2013. Late Cenozoic biostratigraphy of the Linxia Basin, northwestern China. In: Wang

X M, Flynn L J, Fortelius M eds. Fossil Mammals of Asia. New York: Columbia University Press: 243−273

Deng T, Wang S Q, Hou S K, 2013. A bizarre tandem-horned elasmothere rhino from the Late Miocene of northwestern China and origin of the true elasmothere. Chinese Sci Bull, 58(15): 1811−1817

Depéret C, Llueca G, 1928. Sur l'*Indarctos arctoides* et la phylogéne des Ursidés. Bull Soc Géol Fr, Ser 4, 28: 149−160

Frick C, 1926. The Hemicyoninae and an American Tertiary Bear. Bull Am Mus Nat Hist, 56(1): 1−119

Gaillard C, 1899. Mammifäères miocènes nouveaux ou peu connus de la Grive-Saint-Alban (Isère). Arch Mus Hist Nat Lyon, 7: 1−78

Gao Y T et al., 1987. Fauna Sinica, Mammalia. Vol. 8: Carnivora. Beijing: Science Press. 1−377

Ginsburg L, 1999. Order Carnivora. In: Rössner G E, Heissig K eds. The Miocene Land Mammals of Europe. München: Verlag Dr. Friedrich Pfeil. 109−148

Ginsburg L, Morales J, 1998. Les Hemicyoninae (Ursidae, Carnivora, Mammalia) et les formes apparentées du Miocène inférieur et moyen d'Europe occidentale. Ann Paléont, 84(1): 71−123

Goloboff P A, Farris J S, Noxon K C, 2008. TNT, a free program for phylogenetic analysis. Cladistics, 24: 774−786

Heizmann E P J, 1973. Die Carnivoren des Steinheimer Beckens. Paleontographica, Suppl 8(5B): 1−95

Heller F, 1949. Beiträge zur Geologie und Paläontologie des Tertiäres und des Diluviums in der Umgebung von Heidelberg. Sitz Heiderb Akad Wiss, Mat-nat Kl, Abh, 11: 451−508

Hofmann A, 1887. Über einige Säugetierreste aus dem Braunkohle von Voitsberg und Steieregg bei Wies, Steiermark. Jahrb Geol Reichanst, 37(2): 207−218

Hofmann A, 1892. Beiträe zur miocaenen Säugetierfauna der Steiermark. Jahrb Geol Reichanst, 42(1): 63−76

Hunt R M Jr, 1974. The auditory bulla in Carnivora: an anatomical basis for reappraisal of carnivore evolution. J Morphol, 143: 21−76

Hunt R M Jr, 1977. Basicranial anatomy of *Cynelos Jourdan* (Mammalia, Carnivora), an Aquitanian amphicyonid from the Allier Basin, France. J Paleont, 51: 826−843

Hunt R M Jr, 1998. 10. Ursidae. In: Janis C M, Scott K M, Jacobs L L eds. Evolution of Tertiary Mammals of North America, Vol I. Cambridge: Cambridge University Press. 174−195

Jayne H, 1898. Mammalian Anatomy, Part I. The Skeleton of the Cat. London: Lippincott Company. 1−816

Koenigswald G H R von, 1925. Beitrag zur Kenntnis der Gattung *Ursavus* in Schwaben. Centralbl Miner Geol Paläont, Abt B, (1): 16−21

Kretzoi M, 1942. Zwei neue Agriotheriiden aus den ungarischen Pannon. Földt Közl, 72: 350−353

Maddison W P, 1993. Missing data versus missing characters in phylogenetic analysis. Syst Biol, 42(4): 576−581

Marks S A, Erickson A W, 1966. Age determination in the black bear. J Wildlife Manage, 30(2): 389−410

Novikov G A, 1956. Carnivorous Mammals of the Faunas of the USSR. Moscow: AS SSSR. 1−293

Pleijel F, 1995. On character coding for phylogeny reconstruction. Cladistics, 11: 309−315

Qi G Q, 1984. First discovery of *Ursavus* in China and note on other Ursidae specimens from the *Ramapithecus* fossil site of Lufeng. Acta Anthrop Sin, 3(1): 53−61

Qiu Z D, Qiu Z X, 2013. Early Miocene Xiejiahe and Sihong fossil localities and their faunas, eastern China. In: Wang X M, Flynn L J, Fortelius M eds. Fossil Mammals of Asia. New York: Columbia University Press. 142−154

Qiu Z X, Qi G Q, 1989. Ailuropod found from the Late Miocene deposits in Lufeng, Yunnan. Vert PalAsiat, 27(3): 153−169

Qiu Z X, Qi G Q, 1990. Restudy of mammalian fossils referred to Ursinae indet. from *Lufengpithecus* locality. Vert PalAsiat,

28(4): 270−283

Qiu Z X, Yan D F, Jia H, 1985. Dentition of the *Ursavus* skeleton from Shanwang, Shandong Province. Vert PalAsiat, 23(4): 264−275

Schlosser M, 1899. Über die Bären und bärenähnlichen Formen des europäischen Tertiärs. Palaeontographica, 46: 95−151

Scholosser M, 1902. Beiträge zur Kenntnis der Säugetierreste auf den süddeutschen Bohnerzen. Geol Paläont Abh, N F, 5(3): 117−258

Slowinski J B, 1993. “Unorderd” versus “ordered” characters. Syst Biol, 42(2): 155−165

Stehlin H G, 1917. Miocäne Säugetierreste aus der Gegend von Elm (Prov. Hessen). Verh naturf Gesel, Basel, 28: 191−205

Thenius E, 1947. *Ursavus ehrenbergi* aus dem Pont von Euböa (Griechenland). Sitz-ber Akad Wiss Wien, 156: 225−249

Thenius E, 1949a. Die Tortone Säugetierfauna von Neudorf an der March (ČSR) und ihre Bedeutung für die Helvet-Torton-Grenze. Anz Österr Akad Wiss, math-naturw, Kl, 7: 160−171

Thenius E, 1949b. Die Carnivoren von Göriach (Steiermark). Sitz Heiderb Akad Wiss, Mat-nat Kl, Abh, 158(9/10): 695−762

Thenius E, 1979. Zur systematischen und phylogenetischen Stellung des Bambusbären: *Ailuropoda melanoleuca* David (Carnivora, Mammalia). Z Säugetierkd, 44: 286−305

Viret J, 1949. Observations complémentaires sur quelques mammifères fossils de Sobley. Eclogae Geol Helv, 42(2): 469−476

Wang X M, Qiu Z X, 2004. Late Miocene *Promephitis* (Carnivora, Mephitidae) from China. J Vert Paleont, 24(3): 721−731

Wegner R N, 1913. Tertiär und umgelagerte Kreide bei Oppeln (Oberschleisien). Paläontographica, 60: 175−274

Wiley E O, Siegel-Causey D, Brooks D R et al., 1991. The compleat cladist. Univ Kansas, Mus Nat Hist, Spec Publ, 19: 1−158

Wilkinson M, 1995. A comparison of two methods of character construction. Cladisctics, 11: 297−308